ELECTRICAL SWITCHING EFFECTS IN VANADIUM-OXIDE COMPLEXES

Thesis for the Degree of Ph. D.
MICHIGAN STATE UNIVERSITY
RUEY JANG YU
1972

This is to certify that the

thesis entitled

ELECTRICAL SWITCHING EFFECTS
IN VANADIUM-OXIDE COMPLEXES

presented by

RUEY JANG YU

has been accepted towards fulfillment
of the requirements for

Ph.D. degree in E.E.

L. Ward Fisher
Major professor

Date 1/2/72

O-7639

ABSTRACT

ELECTRICAL SWITCHING EFFECTS
IN VANADIUM-OXIDE COMPLEXES

By

Ruey Jang Yu

The electrical properties of oxidized vanadium foils were investigated. One mil thick sheets of vanadium, diced into approximately 1 mm by 1 mm squares, oxidized in air at 475°C for up to one week, and then mounted in a spring-loaded sample holder were found to exhibit reversible, nondestructive, current-controlled switching as well as inductance effects.

From the x-ray diffraction patterns and the conductivity-versus-temperature data, it was concluded that these oxidized samples were in the amorphous state; furthermore, the oxidized layers were not VO, VO_2, V_2O_5, etc. but rather appeared to be a combination of oxide complexes.

The ratio of a typical sample's "off-state" to "on-state" resistance was observed to be approximately 100. The breakdown voltage ranged from 3 volts to 10

volts and was found to decrease as the bath temperature was increased. The delay time for the device to switch was measured and found to be dependent upon the ambient temperature, as well as the magnitude of the applied voltage.

The inductance of a typical sample was found to be strongly dependent upon the dc bias current but independent of frequency, suggesting possible applications as a varactor. For the case of zero dc bias, inductances in excess of 100 mH were observed; however, the Q of the structure was quite low.

An expression for the threshold voltage required for the sample to switch from the low-conductance state to high-conductance state was obtained in terms of the sample's thermal conductivity and rate of change of electrical conductivity with temperature. The expression was found to be basically in agreement with experiments.

The negative resistance of the unit was also observed, and it was shown that the formation of a current channel does not necessarily imply that the material must exhibit negative-differential resistance. Finally, a criteria for observing the negative-differential resistance in current-controlled, bulk-switching devices was established.

ELECTRICAL SWITCHING EFFECTS IN VANADIUM-OXIDE COMPLEXES

By

Ruey Jang Yu

A THESIS

Submitted to
Michigan State University
in partial fulfillment of the requirements
for the degree of

DOCTOR OF PHILOSOPHY

Department of Electrical Engineering
and System Sciences

1972

To My Parents
and
to Suefen

ACKNOWLEDGEMENT

The author wishes to express his sincere appreciation to his major professor Dr. P.D. Fisher, for providing his thoughtful guidance, genuine wisdom and encouragement during the course of this investigation, and also for his painstaking review of this manuscript.

Many thanks also to Dr. K. Subramanian for his encouragement and help in the investigation of the sample's structual properties. He also wishes to acknowledge the other members of the guidance committee, Dr. J. Asmussen, Dr. B. Ho and Dr. D. Montgomery for their time and interest in this work.

Finally, the author wishes to thank his wife, Sue Fen, for her patience, understanding and encouragement in the entire period of his study.

LIST OF CONTENTS

LIST OF ILLUSTRATIONS

FIGURE

FIGURE

FIGURE

LIST OF TABLES

CHAPTER I

INTRODUCTION

During the past two decades, significant progress has been made in terms of understanding the properties of crystalline semiconductor materials. The mathematical treatment and subsequent understanding of these materials has largely depended on the simplification which can be introduced due to the material's periodic nature[1]. However, periodicty is not vital in explaining the electrical properties of all crystals, as can be seen by the fact that no sharp drop in conductivity[2] is observed at the melting point of many materials. At this temperature, long range order in the material disappears, yet the electrical properties are only slightly altered. The early investigation of these rather disordered materials showed only that the electrical conductivity was very low[2]. The study was of interest theoretically as an extension of the study of more highly-ordered, crystalline materials[2].

It was not until around 1960, that significant research activity[1,3,4] was undertaken in order to develop an understanding of the electrical-conduction properties of amorphous, chalcogenide and transition-metal-oxide semiconductors[7]. The interest in these materials was largely due to the discovery that these bulk materials possess switching[3,4] and/or memory effects[7,8,10] as well as negative-differential resistances[11,15,16]. Furthermore, some of the materials were found to possess inductance properties[3]. Because of their unusual and potentially useful properties[6,7], these materials could become the next generation of widely used semiconductor materials.

Nevertheless, the promise of amorphous semiconductor materials can not be realized until their characteristics can be precisely defined and their operation controlled. The theory for amorphous semiconductors is still not well defined[13-15,18,22]. The nature of the change in the material during the switching process has not been established;[1,15] neither has the nature of the memory effect. Evidence is fairly convincing that a structural change occurs in the material at least in the memory switch[1], but whether it is electrically thermally initiated

has not been settled. Böer[9,24], Berglund[3,16] and others[10] have confirmed that the preswitching, nonohmic behavior of amorphous semiconductors has a thermal origin as a result of Joule heating. By using irreversible thermolynamics and totally neglecting effects due to lattice temperature gradients, Ridley[11] has shown that, in the steady state, the current-controlled, negative-differential resistance in a bulk device favors the formation of thermal filaments. The negative-differential resistance in an isothermal system was also discussed by Burgess[26].

The effort of this thesis project has been devoted to studying the electrical conduction, switching and inductance properties of oxidized vanadium foils. These foils[20] have been selected for investigation for several reasons: First, the approach used in sample preparation readily lends itself to existing hybrid, integrated-circuit technology. Secondly, the foils would cost less to produce and would be easier to work with than the reactively-sputtered thin films currently under investigation by other workers[3,17]. Unlike the majority of the materials being studied by others,

vanadium oxide switches states for relatively low bias voltages, when the heat sink is at room temperatures. Finally, since potentially useful inductance effects have been observed in vanadium oxide, we wanted to follow up the work of Berglund and Walden[3] in order to establish the feasibility of utilizing this effect in fabricating useful integrated-circuit inductors.

The inductance effects observed by Berglund[3] and Walden possessed several undesirable properties: The inductance was strongly dependent upon frequency as well as strongly temperature dependent. In addition, a series resistance of one thousand ohms was present at the 6 mA "on-state", bias point. With the intention of providing additional information concerning the effects of bias current on inductance, as well as uncovering possible methods of minimizing some of the undesirable features of the structure investigated by Berglund and Walden[3], we chose to investigate the properties of an alternate sample configuration. Furthermore, we wanted to extend the inductance-versus-bias-current investigation into the preswitching region in order to provide additional insight into the inductance properties of oxidized vanadium.

Böer and Ovshinsky[9,24] solved the governing nonlinear, time-dependent, thermal-transport equation through a Fourier expansion of the sample's temperature $T(x,t)$ into $T(x,t) = \sum_{\lambda} \sum_{\nu} e^{i\lambda x} e^{\nu t}$. Although they arrived at a closed-form expression for the threshold voltage, their analysis has many drawbacks. Most notable is the fact that their analysis is based on the assumption that $\sigma(T) \alpha \exp(\beta T)$ over the entire temperature range of interest, where β is a constant dependent only upon the material chosen. In reality, $\sigma(T)$ need not (and does not) follow this exponential behavior over the entire temperature range of interest. By Taylor expansion of the temperature-dependent, electrical conductivity and with the aid of Laplace transform techniques, we solved the thermal-transport equation, obtaining an analytical expression for the threshold voltage. Our approach, involving a piecewise linearization of $\sigma(T)$, can be readily adapted to a computer analysis, yielding whatever accuracy is required in the determination of the threshold voltage.

The relationship between the observed negative-differential resistance and the formation of current filaments in a current-controlled switching

bulk device is not well defined; therefore, an attempt was made to determine if the observed negative-differential resistance is a necessary condition for the formation of a current channel in a bulk device. The criteria established is developed in Chapter 4.

CHAPTER II

EXPERIMENTAL PROCEDURE AND APPARATUS

2.1 Sample Preparation

Under favorable thermal boundary conditions, many bulk materials, whose electrical conductivity increases significantly with temperature and then becomes saturated above some temperature, will exhibited switching effects when subjected to a certain critical bias voltage. VO_2[3,6], V_2O_3, V_2O_5[17] and chalcogenide glasses[4,15] are examples of materials which exhibit these properties. For vanadium dioxide, the abrupt change in electrical conductivity at 68°C was found[18,19] to be associated with a phase change from a monoclinic to a rutile structure. Futaki[17] observed switching in sintered pellets of VO_2 and Berglund and Walden[3] observed a similar phenomena in reactively-sputtered thin films of VO_2. With their sample configurations in mind, as well as their sample preparation procedures, we elected an alternate approach to prepare our oxidized vanadium samples, a sample preparation techniques and thermal

boundary configuration which proved to offer several advantages over the others.

A pure vanadium foil of [20] 1 mil thickness was diced into 3 mm by 3 mm squares. After cleaning the (TCE), these samples were oxidized in an air atmosphere at temperatures ranging from 300°C to 600°C for periods ranging from a couple hours to one week. The oxidized samples were then taken out of the furnace and abruptly cooled in air.

After many observations, it was concluded that, if the furnace temperature was maintained above 600°C, the resultant samples were very brittle and difficult to handle without fracturing. On the other hand, if the furnace temperature was below 300°C, no matter how long the foil was heated, no significant oxidation occured. Strong evidence indicated that the best furnace temperature for oxidation was around 450°C. At this temperature, it took one week to oxidize foils in order to obtain specimens possessing the desired switching effects. Even after oxidization for one week, chemical polishing showed that only the outer section of the vanadium foil was oxidized, indicating that the oxide layer possibly inhibited oxidation from proceeding past a certain point.

Unless otherwise stated, all data presented in this thesis are for oxidized layers prepared at 450°C for one week.

Once the oxidized vanadium layers were obtained, many of their important properties were evaluated. The rest of this Chapter is devoted to describing the experimental methods used in determining the following properties of the layer: (1) crystalline structure of the layer, (2) dependence of the layer's electrical conductivity on the layer's temperature, (3) the switching delay time under various bias and temperature conditions, (4) the inductance properties of the material, and (5) the effects of large-scale ac signals on the layer.

2.2 X-Ray Diffraction Experiment

The electrical resistivity of the oxidized layer was estimated to be about 10^5 ohm-cm at room temperature. This value is four orders of magnitude higher than that of vanadium dioxide, and is much higher than that of V_2O_3 or V_2O_5 [17,19]. Based on this fact, it is unlikely that the oxidized layer was a simple vanadium-oxygen compound. This should not be surprising since the vanadium foil was heated in the air without any control of the surrounding environment.

If the layer is crystalline, conventional band theory should be able to explain most of the observed electrical effects. If, however, the layer is amorphous, the problem of relating the experimental results to a theoretical model becomes quite complex. In order to determine the nature of the oxide layer a back-reflection, pin-hole, x-ray study was used. This technique is the same as the powder technique, except for the type of the specimen. In the pin-hole technique, sheet specimens are used instead of powder specimen. The x-radiation used is monochromatic.

According to Bragg's law, constructive interference of x-ray will take place when

$$\lambda = 2d \sin \theta,$$

where λ is the wavelength of x-rays, d is the interplanar distance, and θ is the Bragg angle.

This would provide a sharp diffraction maxima (lines) for crystalline materials at the Bragg angle. If the material is polycrystalline, due to the possible random orientations, these diffraction beams will emerge as cones. A film intersecting these cones will show rings, as the pin-hole diffraction pattern. However, the amorphous materials, no such

sharp peaks will exist due to the lack of long range periodicy in the structure. These peaks may be diffused.

The exact experimental configuration used is described in details in Appendix A. It is worth noting here, however, that the majority of the measurements were done on a Strahlenschutzzulassung PTB-526 x-ray machine, and that the x-ray tube was operated at 30kV and 15mA with a typical sample exposure time of 8 hours. The target was copper and a nickel filter was employed, yielding a wavelength of 1.54°A. Results of the x-ray diffraction experiment will be described in the next Chapter.

2.3 Temperature Dependence on Electrical Conductivity Experiments

The electrical conductivity of most metals decreases as the temperature is raised. This is due to the fact that carrier mobility decreases as the result of increasing collisions with phonons, while the concentration of carriers is almost unchanged. On the other hand, for crystalline semiconductors, electrical conductivity always increases as temperature is raised. The increase of electrical conductivity is

due to the increase in the density of free carriers generated from either the impurity bands or valence band by thermal agitation. For most of the amorphous semiconductors, electrical conductivity is more or less temperature, frequency and electrical field dependent as is the case for ordinary crystalline semiconductors; however, the manner in which the conductivity changes is in general different. For example, measurements of the conductivity of amorphous semiconductors as a function of the applied field's frequency shows an increase of conductivity with increasing frequency, in contrast to band conduction which exhibits a slow decrease[31]. Measurements of the conductivity of amorphous semiconductors as function of the applied electric field show that the log of the electrical conductivity varies as the square root of the applied electrical field[31]. Evidence also shows that for temperatures above room temperature, the conductivity of most amorphous semiconductors has the same temperature dependence as that of crystalline semiconductors; however, for sufficiently low temperatures, a variation in conductivity with temperature of most amorphous semiconductors is $\exp(AT^{\frac{1}{4}})$ instead of $\exp(BT^{-1})$, where A and B are constants[31].

All the above information is critical to the determination of the conduction mechanisms and model for amorphous semiconductors. The so-called CFO model is able to explain many of the above mentioned observations[31]. Understanding the temperature dependence of the electrical conductivity of amorphous semiconductors has another significance: the switching effects observed in amorphous semiconductors are critically dependent upon the ambient temperature of the amorphous layer; furthermore, it has been confirmed that the heat generated in the material due to Joule heating plays an important role in the switching process. Ovshinsky[9] observed that the critical voltage required to actuate switching is inversely proportional to the rate of increase of electrical conductivity with temperature. Since the main concern of this research effort is to investigate the switching effects of the oxidized foils at temperatures in the vicinity of room temperature, it is absolutely necessary to understand how the electrical conductivity of the oxidized layer varies with temperature.

The arrangement for measuring the thermal dependent electrical conductivity is indicated in

Figure 2.1. The layer was held by a spring-loaded holder, and the holder was placed inside of a thermos. A thermometer was used to read the layer's ambient temperature. In order to make sure that the temperature distribution inside of the thermos was uniform, as well as to reduce any thermal transient effects, the temperature was not allowed to vary faster than one degree per minute. Also, in order to minimize the possibility of any spurious field effects, the bias voltage across the unit was never higher than 0.1V. This value was far below the threshold switching voltage.

The protection resistor R_p was always chosen to have a comparable resistance to that of the switching device after breakdown. Two multimeters, Fairchild model 7050, were employed to read the potential drop V_s across the unit and the voltage V_p across the protection resistor. The resistance R_s of the unit will be

$$R_s = \frac{R_p V_s}{V_p} , \qquad 2.1$$

and the conductivity of the layer will be

$$\sigma(T) = \frac{L}{A R_s} = \frac{L V_p}{A R_p V_s} , \qquad 2.2$$

where L is the thickness of the oxidized layer, and A is the contact area between the electrode and the layer.

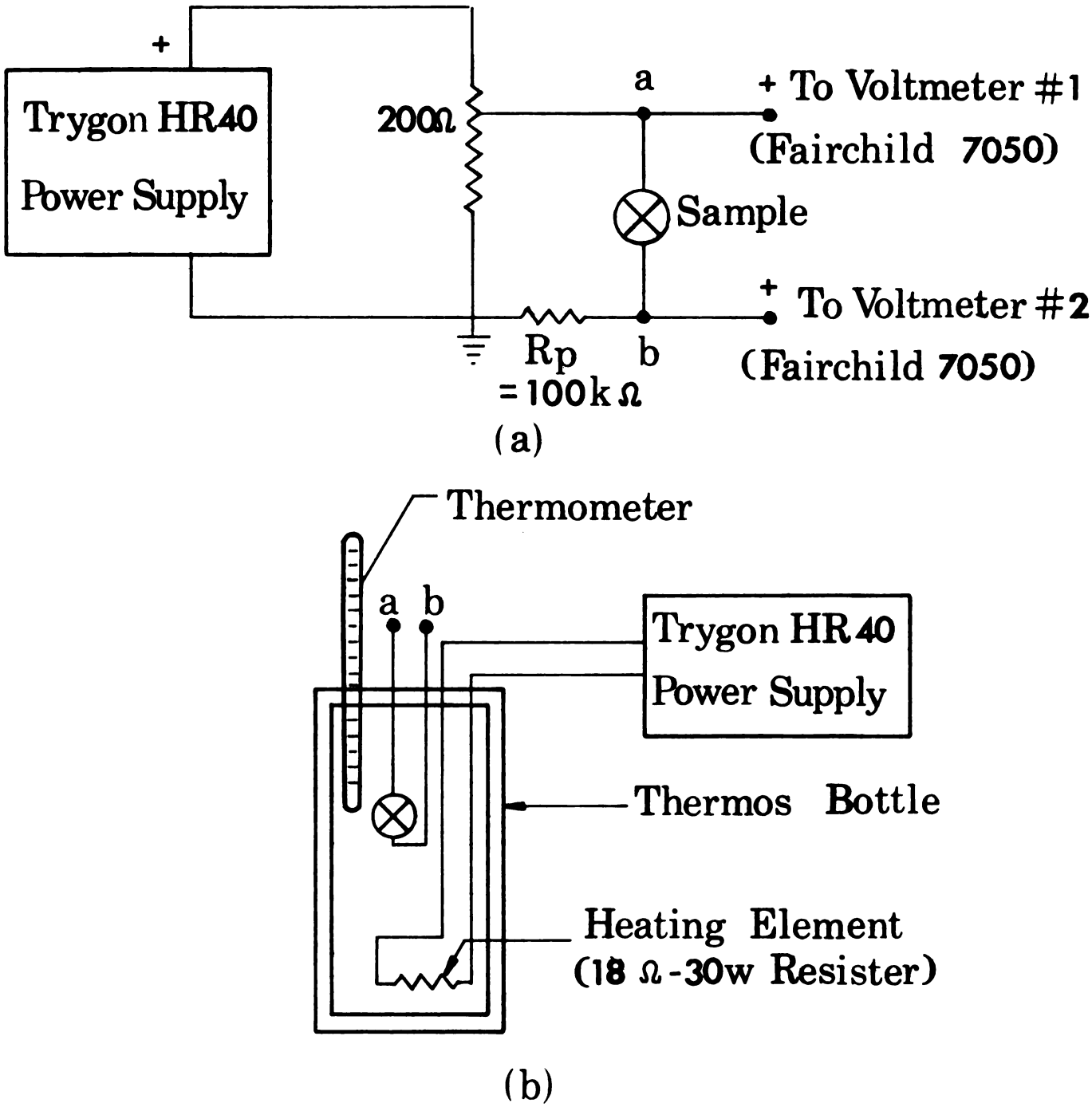

Figure 2. 1. (a) Schematic diagram of the electrical circuit used to measure the resistance of the sample for various bath temperatures. (b) The oven used to heat the samples.

2.4 Switching Delay Time Measurement Procedures

There are several important properties which determine the usefulness of two-terminal, passive switching elements:

1. "Off-state" resistance--The ideal off-state resistance of a two-terminal switch is infinite.
2. "On-state" resistance--The ideal on-state resistance is zero for a two-terminal, resistive-type switch.
3. Switching delay time--The switching delay time is the time delay required for the unit to switch after a command voltage greater than the threshold voltage has been applied. In an ideal switching device, this delay time is zero.
4. Transient time--The transient time of the switching device is the interval of time it takes for the device resistance to change from $0.1(\Delta R_s)$ to $0.9(\Delta R_s)$, where ΔR_s is the difference between the device "off-state" and "on-state" resistance. For an ideal switching device, this time is zero.

5. Threshold voltage or current--The threshold voltage is the voltage required for the device to change states. The desired magnitude of this voltage would depend upon the specific application.
6. Hysteresis effects--Hysteresis effects determine the voltage and current required to maintain the switch in the "on-state" once switching has occured. In many applications, it is desirable that no "holding" voltage or current be required in order to maintain the switch in the on-state.

As to the time duration of the switching process, this may be the time required for the molecules of the material investigated within the thermal filament to reorder their structure. This time also may be affected by the external load resistance and the equivalent circuit capacitances and inductances. The true mechanism underlying this switching action is still uncertain.

The time delay in amorphous-semiconductor, switching devices is apparently[9] related to the time required for the material to reach some critical temperature. Once this critical temperature has

been reached, an unknown thermoelectric process is activated; the state of the material changes abruptly and a current channel forms inside the layer. Since certain applications may arise which require hundreds of switching elements to perform a single function, if the switching delay time and the transient time of each composite switching element is too long, the total switching time for the system would be prohibitively long.

From many observations of the investigated layer, it was concluded that the transient time is much-much shorter than the delay time required for the switching action to occur. Hence, the total switching time is limited by the delay time. This is consistent with many reports from other workers who have observed[4,15] the transient time in various amorphous switching elements to be around 10^{-9} second. Since one of the main concerns of this research effort is to investigate the preswitching behavior of the oxidized vanadium foils and to determine the limitations on the various switching properties, the time delay for the unit to initiate switching after the application of the command signal must be thoroughly investigated in order to determine exactly what practical limitations are placed on this delay time.

The experimental arrangement for measuring the delay time as a function of both ambient temperature and applied voltage is depicted in Figure 2.2. The layer was held by a spring-loaded holder and was placed inside of a thermos so that the ambient temperature of the device could be closely controlled. A repetitive voltage step was applied to the device. The switching delay time was measured by comparing on a Tektronix Type 851A, dual-trace oscilloscope the input signal with the system response. Using this arrangement, the dependence of delay time on ambient temperature and applied voltage was determined. Results of this investigation are presented in the next Chapter.

2.5 Inductance Measurements

Inductance effects have recently been observed by Berglund and Walden[3] in sputtered, vanadium-dioxide, thin films. All of their inductance measurements were made well above the switching threshold. Although they observed inductances on the order of 10mH for a 6mA bias, their thin-film inductors possessed several undersirable properties: The inductance was strongly dependent upon frequency as well as strongly temperature dependent. In addition, a series resistance of over

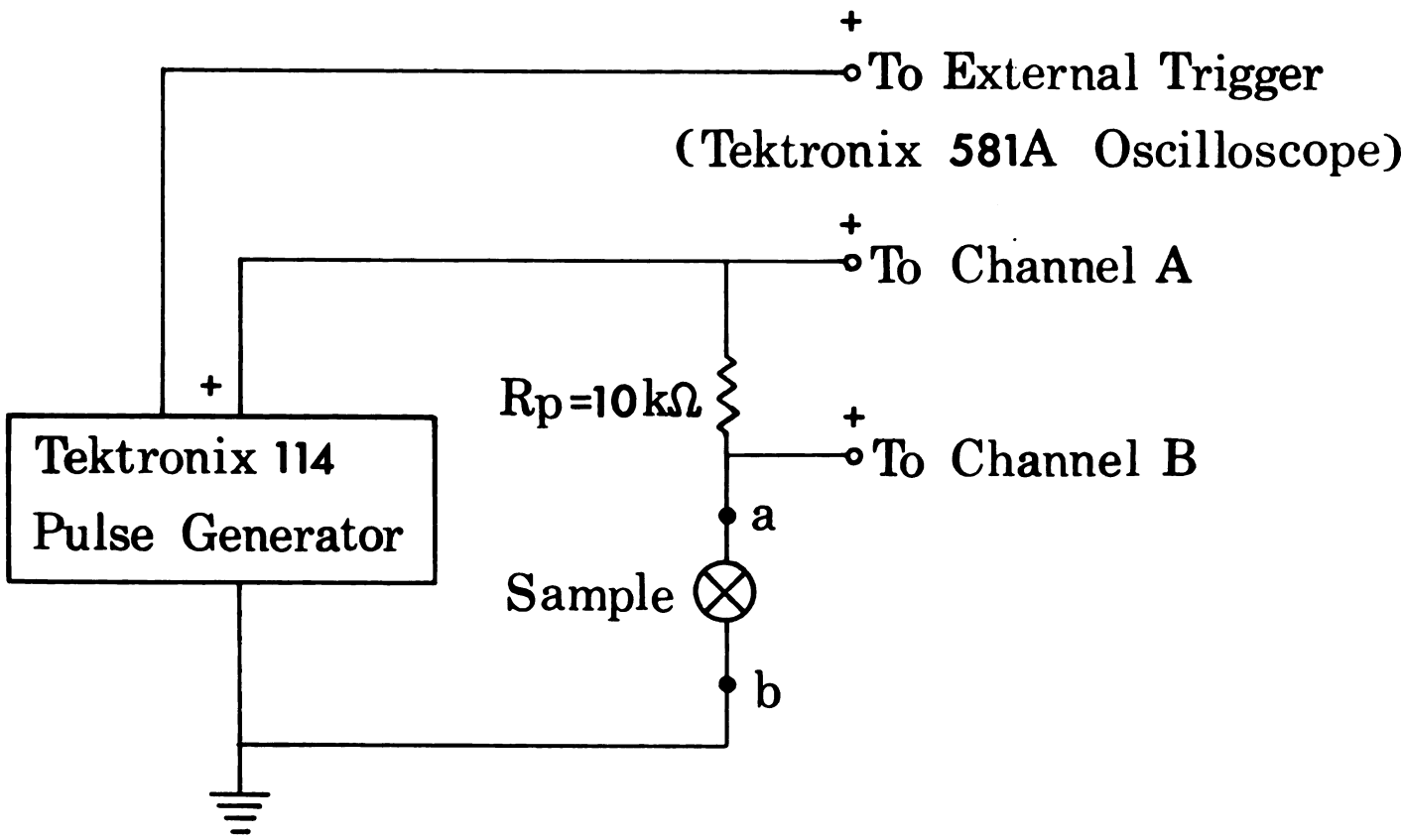

Figure 2. 2. Schematic diagram of the electrical circuit used to measure and display on an oxcilloscope the switching delay time for various sample temperatures. The oven arrangement is the same as that depicted on Figure 2. 1.

one thousand ohms was present at the 6mA bias point. All of their results were successfully explained in terms of the thermal-transport properties of the material.

Inductance is an important electrical property of an electrical element. The inductance may be detrimental to a switching device because it is a parasitic parameter which may severely degrade the switching time. On the other hand, in steady-state, ac applications, high Q inductors are always a welcome cirucit element, particularly if the inductive element is compatible with integrated circuit technology. The inductance properties exhibited by the layer investigated thus have far reaching significance in the modern integrated-circuit applications.

With the intention of providing additional information concerning the effect of the bias current on inductance, as well as uncovering possible methods of minimizing some of the undesirable features of the structure investigated by Berglund and Walden[3], an experimental investigation of these inductance properties was undertaken.

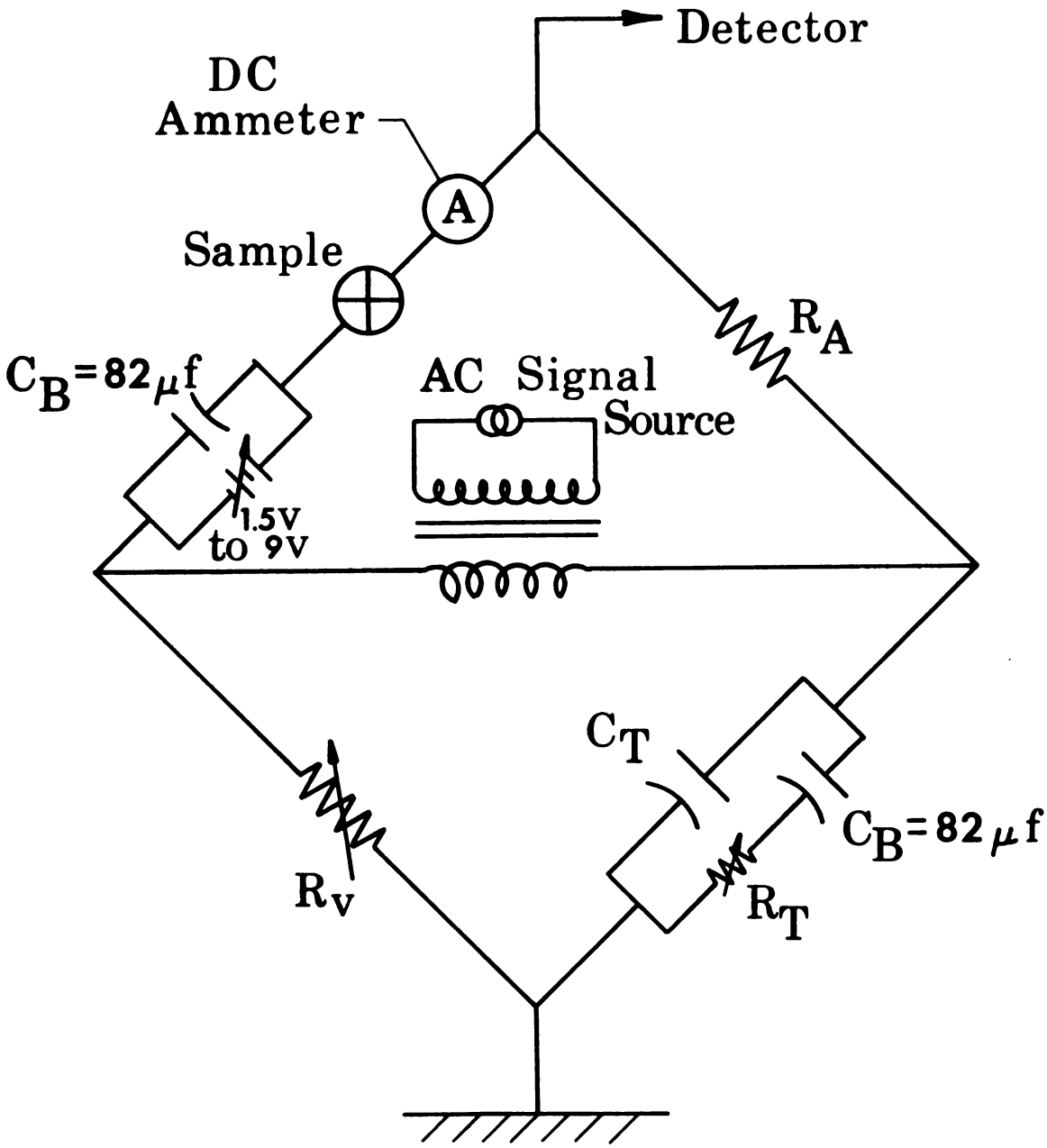

Figure 2. 3. Modified GR1650A bridge used in measuring the impedance of the samples.

Two oxidized foils, with one side of each chemically polished and silver painted, were sealed to electrodes of the sample holder. The electrodes were much more massive than the layer; consequently, they served as infinite heat sinks. Since the inductance of the sample was affected by both the dc current flowing through the layer and ac signal frequency, a systematic method of measuring the layer's inductance under various dc current and ac signal frequency was employed. By using a modified General Radio Type 1650-A Impedance Bridge, the dc bias current I_B was varied from 0 to 15 mA. The ac signal current I_S was held constant at approximately 100μ A, while the frequency of the ac signal was varied from 100 Hz to 25 kHz, the approximate normal operating range of the bridge. The circuit employed is depicted in Figure 2.3. All inductance measurements were made at room temperature. Results of the investigation are described in the next Chapter.

2.6 Experiments Of Response To 600-Hz Large-Scale Signals

An electronic switching device would be a very limited use if its properties change permanently as a result of the switching action. An experiment was designed, therefore, to evaluate the effects of many

switching cycles on the properties of these oxidized layers.

The experimental arrangement is indicated in Figure 2.4. The peak value of the input potential was 9 volts, which is a little higher than the layer's threshold voltage at room temperature. A sinusoidal voltage was applied continuously to the unit over the period of several days without noticable changes taking place in the device's electrical characteristics. It is concluded from this experiment that the switching effect exhibited by the layer is non-destructive.

Detailed results of this aspect of the investigation are presented in the next Chapter.

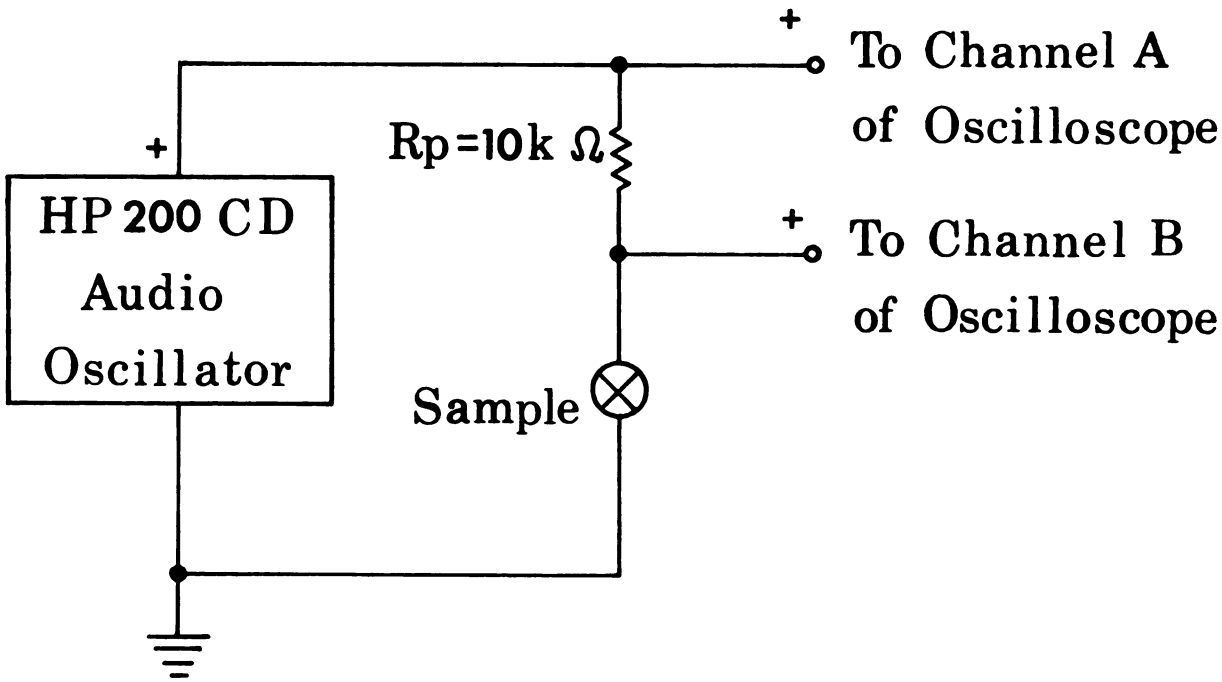

Figure 2.4. Schematic diagram of the electrical circuit used in evaluating the useful lifetime of devices when the devices are under the stress of continuous, large-scale, AC signals.

CHAPTER III

EXPERIMENTAL RESULTS

3.1 Structure Properties of the Unit

Figure 3.1 shows the back-reflection, pin-hole x-ray diffraction photograph of a pure vanadium foil. A broken ring of radius 22 mm shows up, indicating that the vanadium foil is polycrystalline. The magnitude of the radius of this ring is what we expect for polycrystalline vanadium. Figure 3.2 shows the x-ray picture of the oxidized vanadium foil. In this photograph, no such ring is present; on the contrary, the whole central zone of the film appears to be exposed. This strongly suggests that no sharp, coherent reflections of the incident x-ray beam took place, indicating that the oxidized layer was amorphous. Figure 3.3 shows another x-ray picture of another oxidized vanadium foil; a ring with a radius of 30 mm is present, as well as the hazy background evident in Figure 3.2. This photograph was taken using a different x-ray machine, different oxidized vanadium foil, and different distance between the film and the object, but otherwise under identical conditions. This ring was confirmed to be the result of the sharp coherent

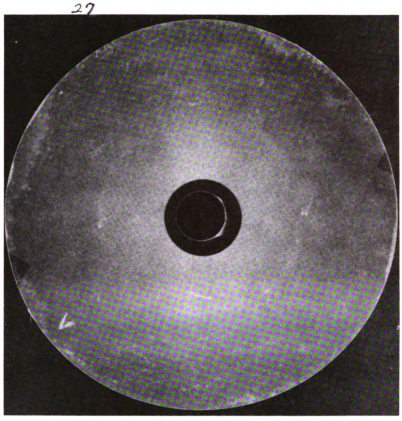

Figure 3. 1. Back-reflection, x-ray pattern for a pure vanadium foil.

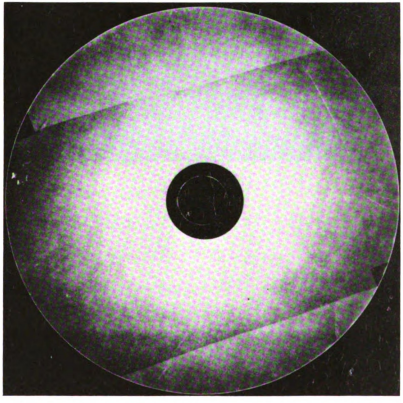

Figure 3. 2. Back-reflection, x-ray pattern for an oxidized vanadium foil, illustrating the amorphous nature of the oxide layer.

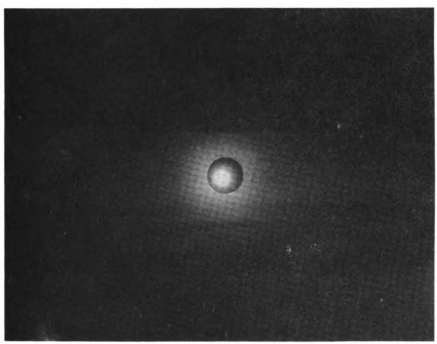

Figure 3. 3. Back-reflection x-ray pattern for the oxidized vanadium foil, illustrating the presence of both the amorphous oxide layer and the pure-vanadium foil beneath the layer.

diffraction of the incident x-ray by the pure vanadium, indicating that the foil was not completely oxidized. This is not surprising since the oxidized layer was estimated to be around 1 micron thick. The incident x-rays penetrated through this thin layer and got reflected by the inner unoxidized material. Besides this ring, which can be directly attributed to pure vanadium, no other rings are observed in the photograph. This suggests that the oxidized vanadium layer was in the amorphous state.

The oxidized layer will be primarily an assortment of vanadium-oxygen complexes. There will be a negligible amount of nitrogen-vanadium and hydrogen-vanadium complexes present in the layer because the solubility of hydrogen and nitrogen in vanadium at 475°C is very low[32-34].

3.2 D.C. Conductance

Typical electrical conductance of the layer in the temperature range from 25°C to 100°C is shown in Figure 3.4. As indicated, the electrical conductance is strictly an increasing function of ambient temperature in the above mentioned temperature range. This behavior can be approximated by the expression

$$\sigma(T) = \sigma_o \exp \beta(T-T_o) \qquad 3.1$$

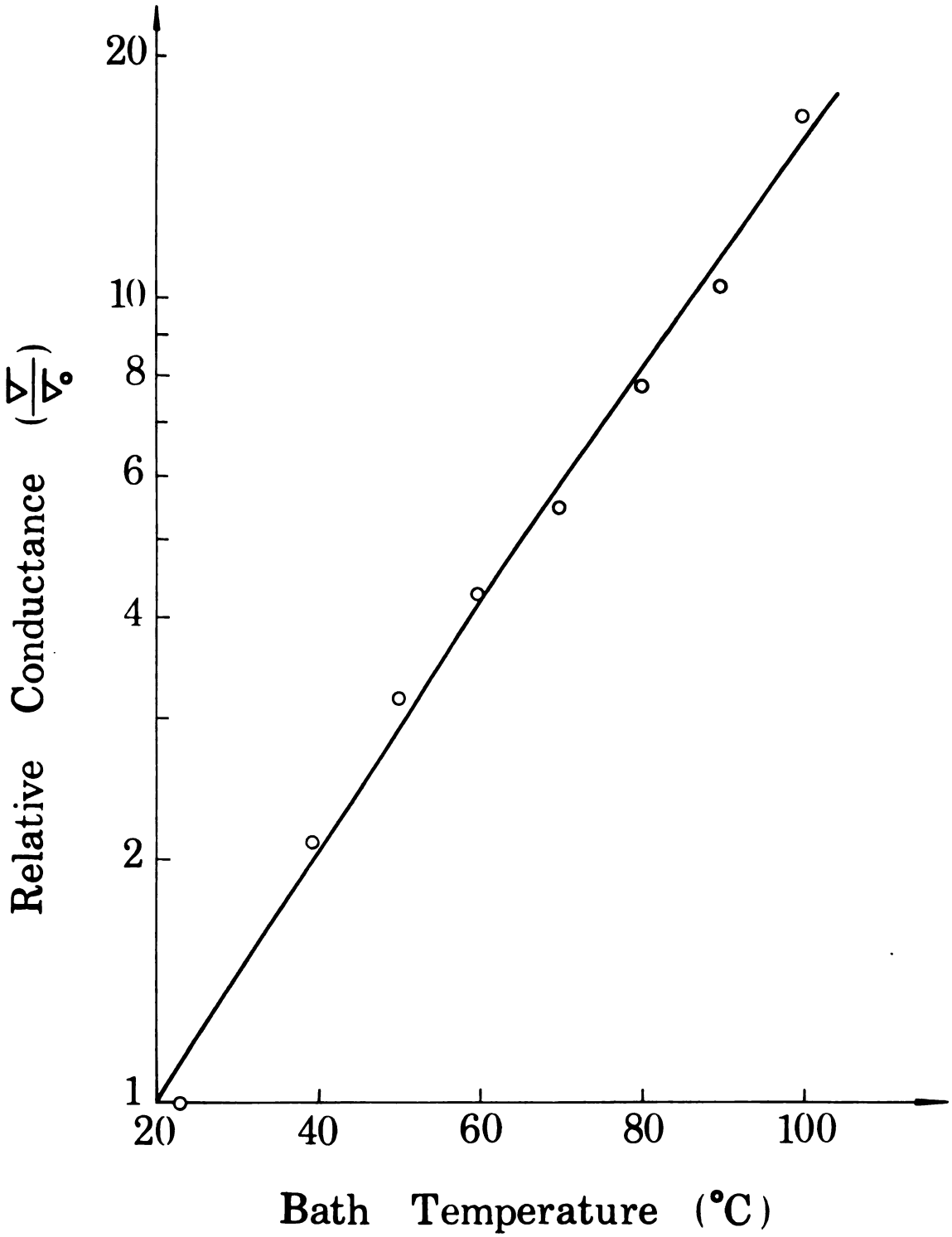

Figure 3.4. Temperature dependence of a typical oxidized vanadium foil's conductance. $V_{BIAS} << V_c$.

for T near T_o, where T_o is the ambient temperature, $\beta = \frac{\Delta E}{kT^2}$, and ΔE is the introduced energy-gap-like quantity. ΔE is strongly temperature dependent and is estimated to be around 0.3 ev at room temperature for the layer investigated.

Since pressure exerted on the oxidized layer by the spring-loaded electrodes will alter the layer's energy gap and thus its conductivity, all the conductivity measurements were made under the same pressure of 12 pounds per square inch.

Another approximation made in all the measurements was that the junction resistance between the layer and electrodes was negligible and independent of temperature. This is because contacts were ohmic and independent of the contact materials. This ohmic behavior of the contacts can be explained by tunneling through electrode barriers of small screening length in highly disorder materials[7].

As mentioned earlier, conductivity is affected by the strength of the applied electric field. If the bias voltage is far below the threshold value, the field effects will only be minor.

In Figure 3.5, the temperature dependence of threshold voltage V_C, threshold current I_C and threshold power P_C required for the unit to actuate switching in the temperature range from 25°C to 100°C is summarized. Also shown in the temperature dependence of holding voltage V_H and holding current I_H for the unit to sustain its "on" state. From this Figure, it is obvious that the threshold current I_C is almost temperature independent, while the threshold voltage V_C drops down almost linearly with increasing temperature. The explanation of this is that the higher the ambient temperature, the smaller the incremental temperature increase required to bring the layer to the critical temperature T_C, where T_C the temperature required for the layer to switch states; also, the higher the ambient temperature, the higher the temperature rate of the increasing electrical conductance of the layer; consequently, as the ambient temperature increases, P_C and V_C decrease, the amount of decrease being strongly dependent upon the thermal boundary configuration. An analytical expression relating threshold voltage V_C and the bath temperature will be developed and discussed in the next Chapter.

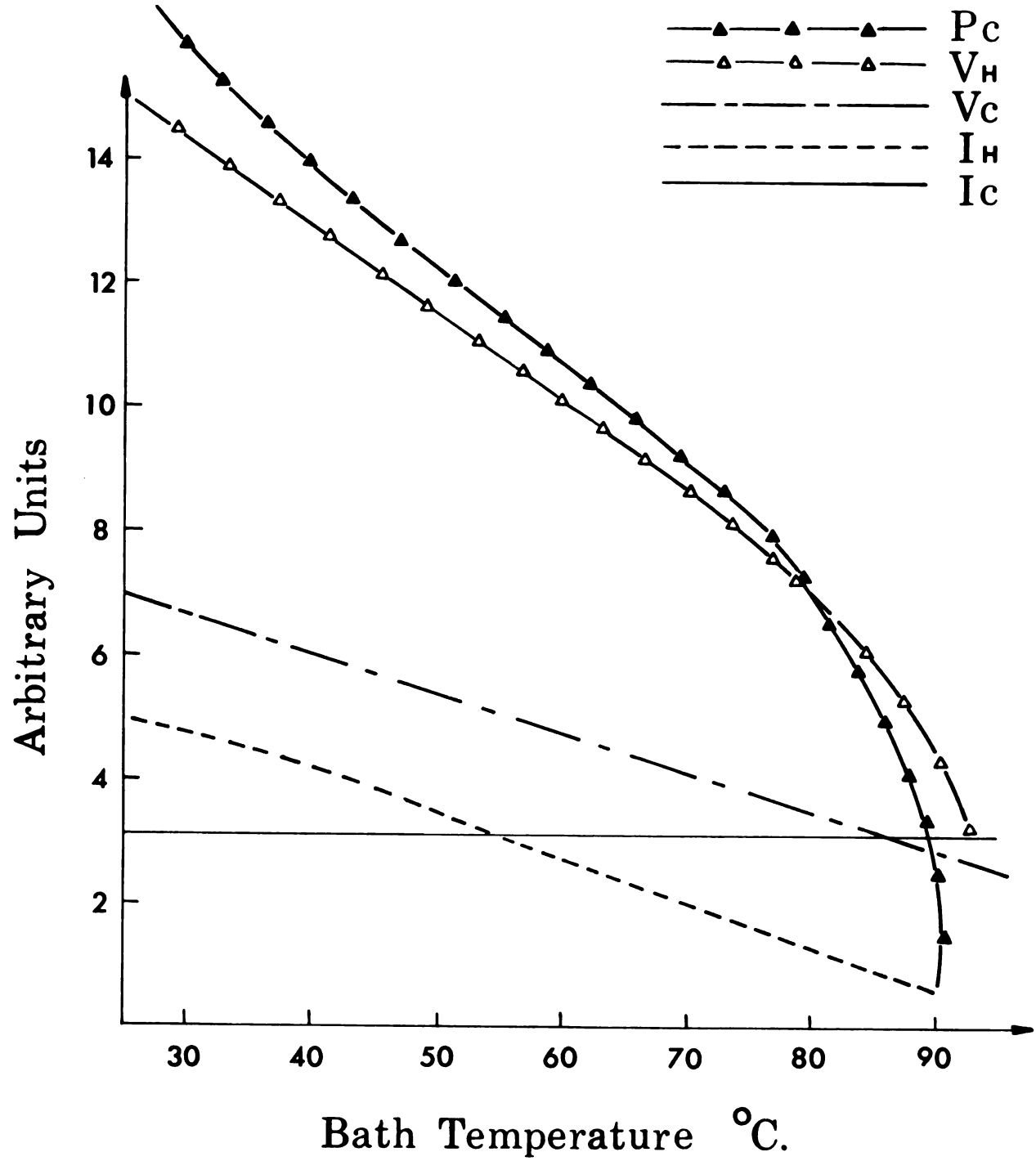

Figure 3.5. Temperature dependence of a typical sample's threshold current Ic, threshold voltage Vc, threshold power Pc, holding voltage VH and holding current IH.

3.3 Typical I-V Characteristic Curves

A typical characteristic I-V curve is shown in Figure 3.6. The main features of the switching phenomena shown are the following: (1) The I-V characteristic is symmetrical with respect to the reversal of the applied voltage and current. (2) The same symmetrical switching characteristic is sustained when the electrodes are of different contacting area or of different materials. However, as the contact area is changed, the critical voltage and current and holding current and voltage may change. (3) In the highly resistive "off" state, the material is ohmic, as the bias voltage increases from zero up to some critical value. The typical resistance of the unit in this region is around 10 kohm. (4) When the applied voltage exceeds the threshold voltage V_C, the unit switches along the laod line to the conducting state. During this transitional state, negative resistance sometimes is evident. (5) In the conducting "on" state, the current can be increased or decreased without significantly affecting the voltage drop, termed the holding voltage V_H. In this "on" state, the dynamic resistance is quite low (around 100 ohms). Typically the on-off resistance ratio

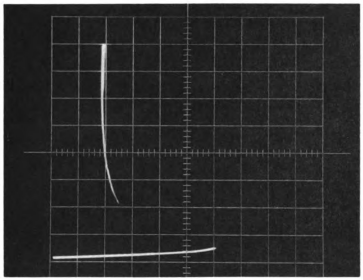

Figure 3.6. Typical I-V characteristic curve of an oxidized vanadium layer. Horizontal scale is 1V/div, and the vertical scale is 1mA/div. Bath temperature is 24° C.

is around 100. (6) As the current is reduced below a characteristic value termed the holding current I_H, the unit rapidly switches to the original high resistive state along the laod line. (7) The switching process is repeatable. A series of pictures showing the ambient temperature effects on the I-V characteristics are given in Figure 3.7. The protecting resistance in taking these I-V characteristic curves was 200 ohm. The pictures were taken at ambient temperatures 25°C, 35°C, 45°C, 55°C, and 60°C respectively. From this experimental data, it is obvious that the threshold voltage is strongly temperature dependent while the critical current is essentially temperature independent. Reasons for this behavior will be extensively discussed in the next Chapter.

3.4 Switching Delay Time Constant

The response of a typical oxidized vanadium layer to a square-wave voltage of various amplitudes is shown in Figure 3.8. All the experiments were performed at 23°C; the protecting series resistance was 10 kohm in each case. It was found that the higher the bias voltage, the shorter the delay time required for the layer to switch. Typical data

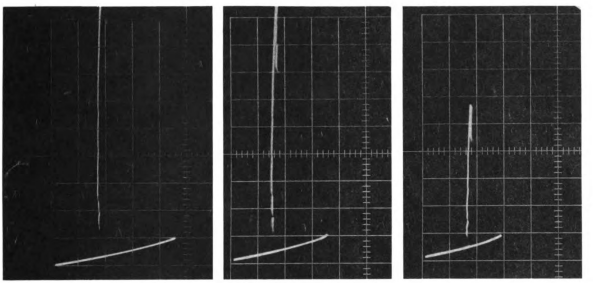

a b c

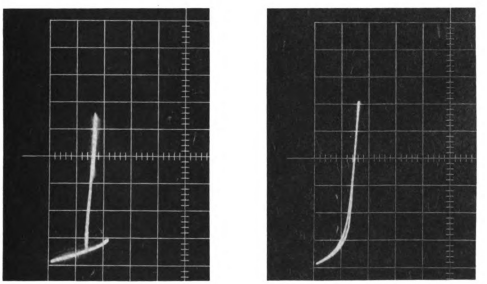

d e

Figure 3.7. I-V characteristics for a typical sample at (a) 23° C, (b) 35° C, (c) 45° C, (d) 50° C and (e) 60° C. Horizontal scale is 1V/div, and the vertical scale is 1mA/div.

Table I

Delay Time Data for Various Applied Voltages as Depicted from Figure 3.8.

Voltage Applied (Volts)	Delay Time (Microsecond)
4.7	10
4.8	8
5.1	6
5.6	4

Table II

Delay Time Data for Various Ambient Temperatures as Depicted from Figure 3.9.

Ambient Temperature (°C)	Delay Time (Microsecond)
26	7.0
30	4.5
60	4.0

depicted from the series of pictures are tabluated in Table I

It was also anticipated that the delay time should be strongly affected by the ambient temperature. Figure 3.9 confirms this fact. Here once again the protecting resistance was 10 kohm. From the oscilloscope traces shown, one observes that the delay time decreases with increasing ambient temperature. Results are tabulated in Table II.

Figure 3.10 shows another oscilloscope trace of the response of the sample to the same square wave excitation except that a protecting resistance of 1 kohm is used instead of 10 kohm. Comparing Figure 3.8 with Figure 3.10, one notices that the delay time of the investigated oxide layer in the former case is much longer than that in the latter case. This can be explained as follows: If R_s is the equivalent series resistance of the oxide layer, R_p the protecting series resistance and $e(t)$ the applied square wave potential across both R_s and R_p, then the instantaneous power $p(t)$ dissipated in the oxide layer will be

$$p(t) = \left(\frac{e(t)}{R_s+R_p}\right)^2 R_s = \frac{e(t)^2}{R_s} \frac{1}{(1+R_p/R_s)^2} \qquad 3.2$$

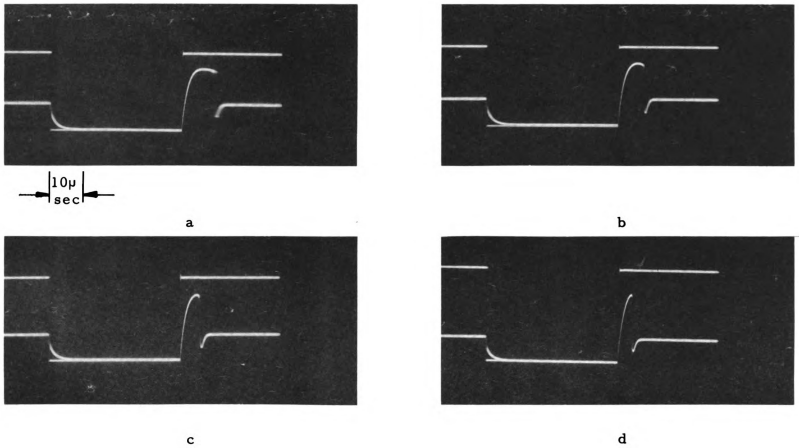

Figure 3.8. Response of a typical, oxidized vanadium layer to a square-wave voltage. The amplitude of the input signal is (a) 4.7 V, (b) 4.8 V, (c) 5.1 V and (d) 5.6 V. Horizontal scale is 10 μ sec/div.

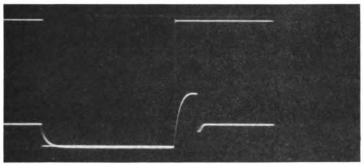

a

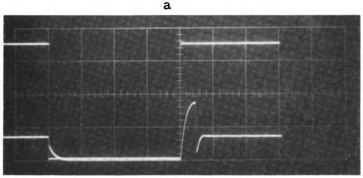

b

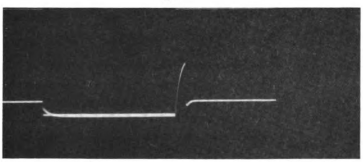

c

Figure 3.9. Responses of a typical, oxidized vanadium layer to a square-wave voltage for both temperatures (a) 26° C, (b) 30° C and (c) 60° C. Horizontal scale is 10μ sec/div, and the vertical scale is 2.5 V/div.

Equation 3.2 implies that for a fixed value of R_s, the instantaneous power dissipated in the oxide layer will decrease as R_p in increased. For a typical oxide layer investigated, R_s was around 10 kohm, while R_p employed in obtaining Figure 3.8 and 3.10 was 10 kohm and 1 kohm respectively. It is obvious that there will be more power dissipated in the oxide layer for the case depicted in Figure 3.10; consequently, the delay time for the oxide layer to reach the critical temperature in order to actuate switching will be shorter for the case of Figure 3.10. This fact lends direct support to the proposed theory that the observed preswitching behavior has a thermal origin.

3.5 Response to A.C. Signals

The input signal is of 600 Hz with peak amplitude of 9 volts as shown in Figure 3.11a. The response of the unit to this signal at room temperature is shown in Figure 3.11b. It was found that the unit investigated can stand millions of switching cycles without noticable changes in its electrical characteristics.

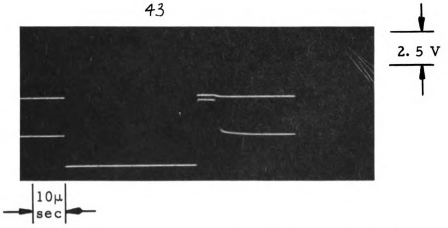

Figure 3. 10. Response to a square-wave voltage for a bath temperature of 26° C with a protection resistor R_1=1kΩ instead of the normal 10kΩ.

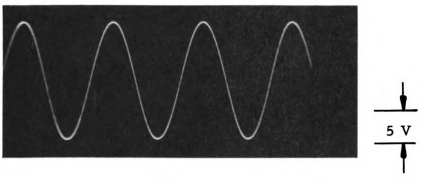

a

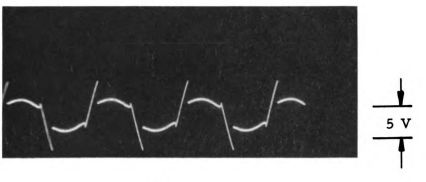

b

Figure 3. 11. Response of a typical sample to a large-signal, 600 Hz applied voltage. (a) Input-voltage waveform, and (b) corresponding voltage drop across the sample.

3.6 Inductance Properties

The inductance effects observed by Berglund and Walden[3] in sputtered, vanadium dioxide thin films were strongly dependent upon frequency as well as temperature. All their inductance measurements were made well above the switching threshold, and were on the order of 10 mH for a 6 mA bias. Since the switching and the inductance properties of amorphous semiconductors are a direct consequence of the material's thermal properties, and since the temperature of any volume element is strongly dependent upon the element's thermal boundary conditions, the thermal boundary of the material as a whole play an important role in ultimately establishing the gross electrical properties of the material.

The ac electrical properties of oxidized vanadijm layers were measured as a function of both frequency and dc bias current using a modified General Radio Type 1650-A Impedance Bridge. The ac signal current I_s was held constant at 100 microampeves, while the frequency of the test signal was varied from 100 Hz to 25 kHz, the approximate normal operating range of the bridge. Inductance versus frequency data for various dc bias levels

is given in Figure 3.12. In Figure 3.13, the effect of dc bias current on inductance is illustrated. The ac series resistance R_s versus frequency data and bias current data are illustrated in Figure 3.14 and Figure 3.15 respectively. It was found that the ac series resistance R_s, like the inductance, was strongly dependent upon the bias point but independent of frequency. It proved to be very difficult to make any inductance or ac series resistance measurements for bias currents between 0.3 mA and about 4 mA because when the load line was adjusted so that the bias current would be stable between 0.3 mA and 4 mA, the Q of the circuit was too low to make meaningful measurements. Berglund and Walden[3] proved that if the thermal hysteresis effects were absent, one would expect the inductance to be independent of frequency. For the sample investigated, no noticable thermal hysteresis effects were independent of frequency.

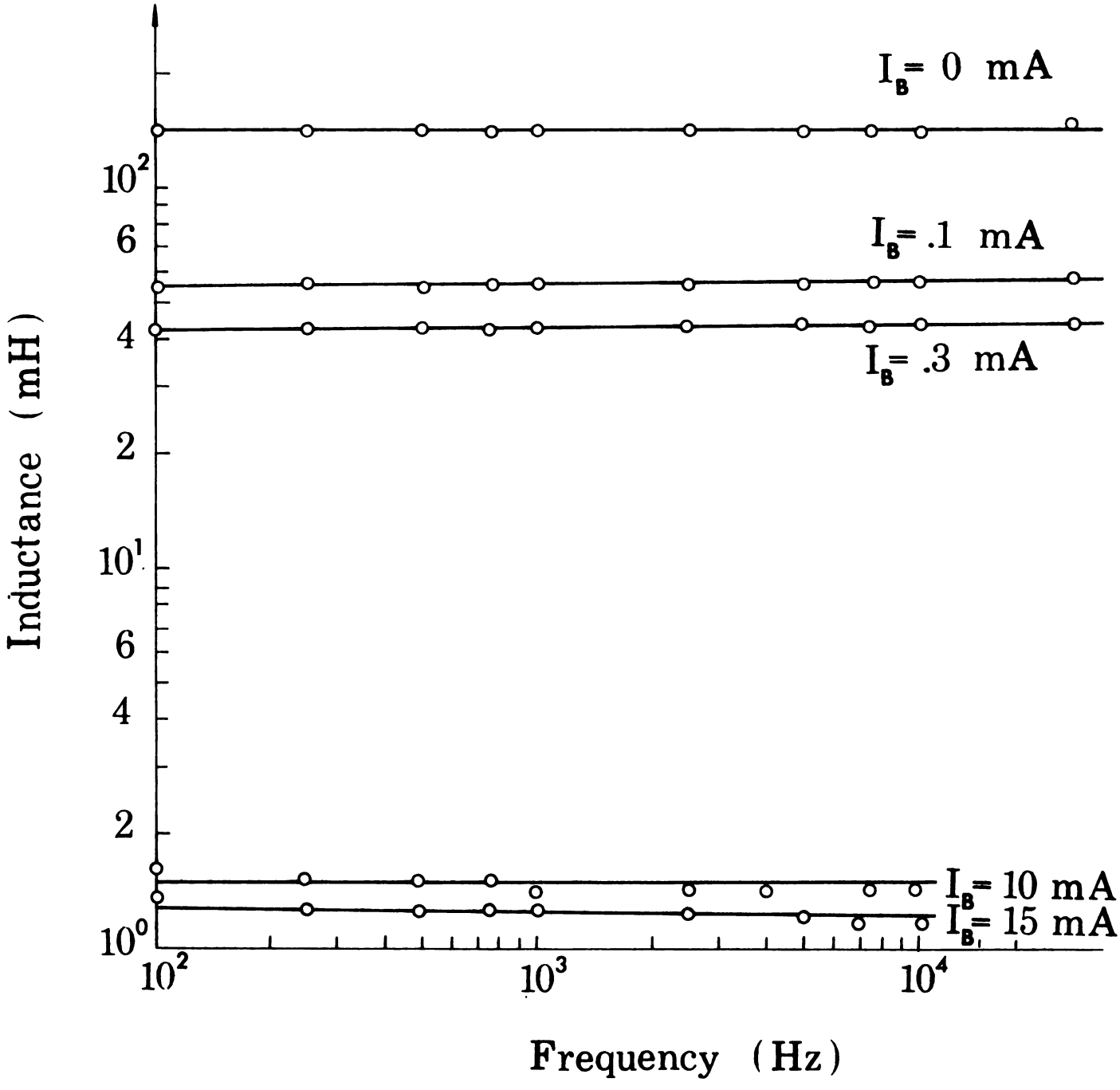

Figure 3. 12. Frequency dependence of inductance for various dc bias currents.

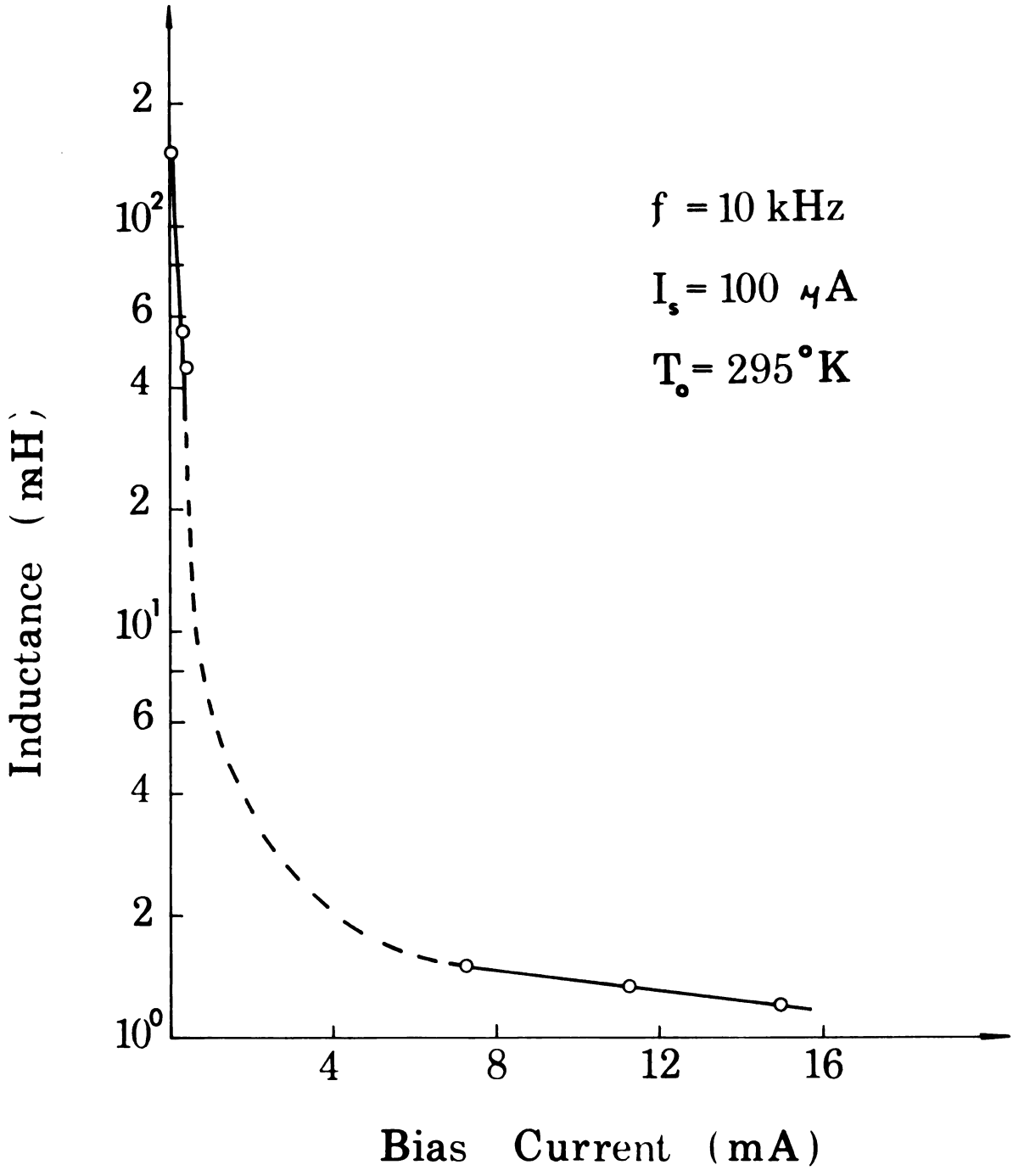

Figure 3.13. Dependence of inductance on dc bias current.

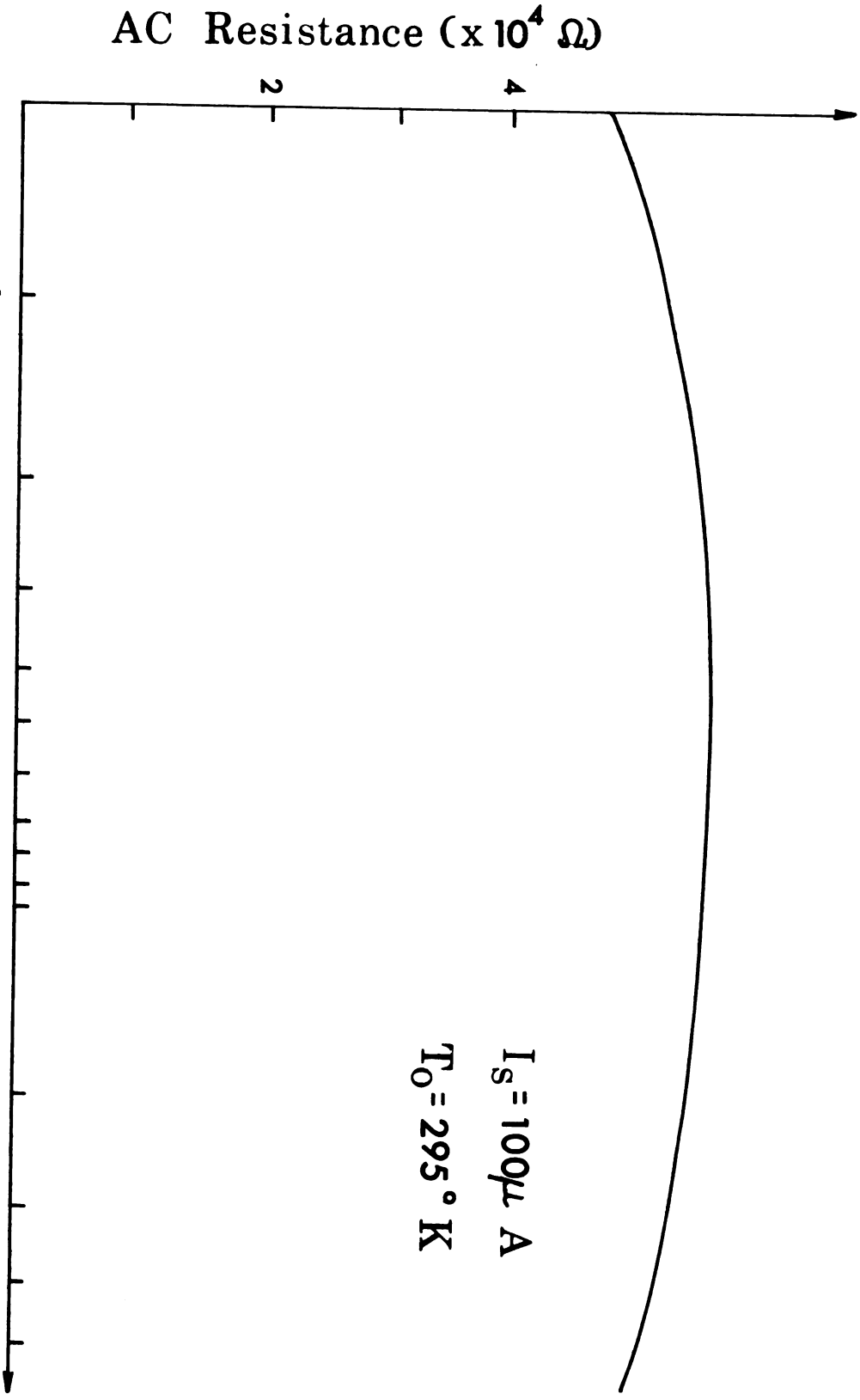

Figure 3.14. Frequency dependence of the small-signal, AC, series resistance.

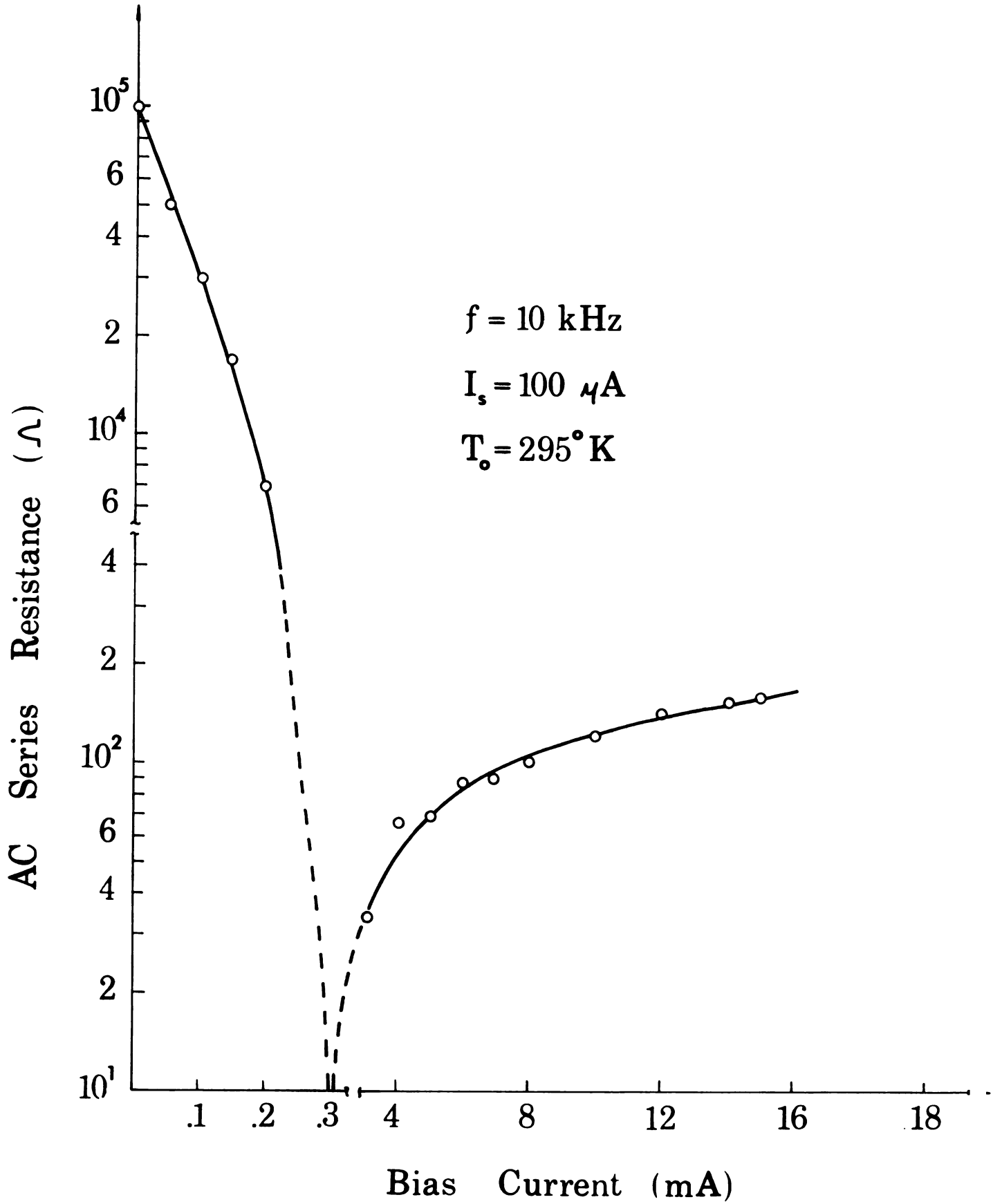

Figure 3. 15. Dependence of the small-signal, series resistance on dc bias current.

CHAPTER IV

INTERPRETATION AND DISCUSSION

4.1 Introduction

Ovshinsky[4] and Walsh[8] have shown that small samples of certain chalcogenide glasses may be made to switch reversibly from a low-conductance state to high-conductance state through the application of a voltage above a certain critical value. Berglund[3] also found that vanadium dioxide films undergo a phase change at 68°C and can be made switch if the bias voltage is above a certain critical value. Böer and Ovshinsky[9] have indicated that the preswitching nonohmic behavior may arise from Joule heating within the material and that the switching is a current-controlled thermal breakdown. Joule heating causes the temperature in a semiconductor to rise. Under usual circumstances, the temperature increase will be stable when the heat generated is balanced by the heat dissipated. Since the temperature profile is determined by the geometry of the semiconductor and its surroundings, the threshold voltage required for the device to generate enough heat and therefore bring about thermal breakdown will be strongly configurational dependendent.

Generally there are three principal types of thermal boundary configurations currently employed by most observers; these are depicted in Figure 4.1. Futaki used the Pellet Configuration in investigating the conductivity versus temperature properties of sintered pellets of various vanadium oxide complexes[17]. Materials investigated using this geometry would be expected to evidence large thermal transient effects due to the relatively poor contact made by the sample and the heat sink. The Planar Configuration was employed by Berglund and Walden[3]. For this geometry, moderately good thermal contace can be made with the heat sink provided the thickness of the sample and the electrical insulating layer between the sample and the heat sink are made sufficiently small.

Ovshinsky, et al. have investigated the electrical properties of various amorphous chalcogenides using the Sandwich Configuration[9]. Because of the direct contact made by the sample with the metal electrodes, this configuration affords the best possible thermal boundary conditions in terms of guaranteeing minimum thermal transient effects. The presence of the high-conductance, low-field "on state" is not entirely due to thermal effects; however, the

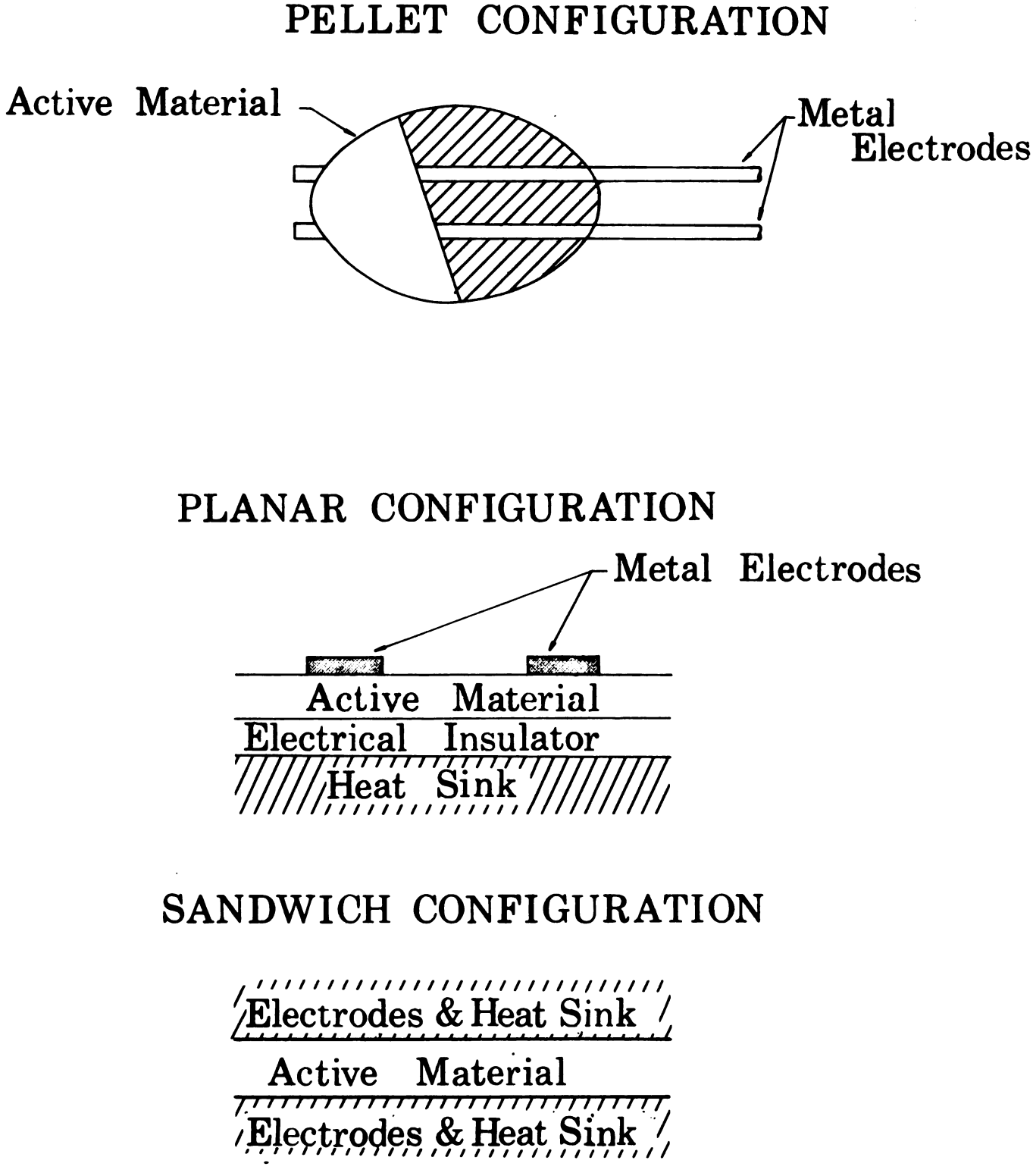

Figure 4. 1. Three possible thermal-boundary configurations.

rapid and reversible transition between the highly resistive and conductive states can have a thermal origin from Joule heating of a current channel.

In the next section (Section 4.2), the thermal transport equation governing the temperature distribution within the oxidized vanadium layer will be solved subject to boundary conditions appropriate to the sandwich configuration. An expression for the critical field required to actuate switching from the low-conductance state to high-conductance state at various bath temperatures is obtained. This expression for the critical field is then compared with experimental results.

In Section 4.3, the technique and approximation made in the analysis of the Sandwich Configuration is extended to the planar configuration. The threshold electric field requires for this configuration to actuate switching is also obtained and discussed.

In the last section (Section 4.4), by totally neglecting the effects due to transverse temperature gradient as did by most observers[11,26], a criteria for observing current-controlled, negative-differential resistance in a bulk, thin-film devices employing

the planar configuration is established and discussed.

4.2 Temperature Distribution and Switching Threshold Voltage of the Device--Sandwich Configuration

4.2.1 Geometry

The first structure of interest (Figure 4.2) is a thin, semiconducting sandwich of comparatively infinite extension in the sandwich plane to the thickness of the sandwich layer, having the temperature dependence of conductivity given by Equation 3.1. This configuration has gained significant popularity recently since the results can be applied to the DO7-Ovonic threshold switch (OTS)[9]. The electrical conductivity, specific thermal conductivity and specific heat capacity of the semiconducting layer and electrodes are σ_s, k_s, c_s and σ_d, k_d, c_d, respectively. The temperature distribution in the semiconducting layer of thickness L_s and that in the two highly conductive electrodes are determined by solving the thermal transport equation

$$c \frac{\partial T}{\partial t} - \text{div}(k \text{ grad } T) = \bar{J} \cdot \bar{E} \qquad 4.1$$

where $\bar{J} \cdot \bar{E}$ is the heat production rate and, $\bar{J}$ and $\bar{E}$ are current density and electric field within the sample respectively. This source term was

balanced by two others, $C\frac{\partial T}{\partial t}$, the heat accumulation rate and, div(kgradT), the rate of heat energy conducted away to the bath through the sandwich and highly conducting electrodes. No heat radiation is concerned here. Since what is of interest here is the preswitching behavior of the oxidized layer before any thermal filament is formed, and since the dimensions of the sandwich plane in both y and z directions are much larger than the thickness L_s of the sample, it is reasonable to neglect all thermal inhomogeneties within the sandwich plane and consequently only the relevant x-direction (normal to the contact area) in Equation 4.1 need be considered. The origin of this coordinate (x=0) shall be at the center plane of the sandwich (Figure 4.2). For simplicity, all bulk property parameters k_i, C_i (i=s,d) will be assumed spatially constant and field, temperature independent. The electrical conductivity σ_d of the electrodes will be so high that no significant Joule heat is generated inside. Also the electric field E inside of the sandwich layer will be assumed space-independent, since space charge effects will be neglected. Thus, the thermal balance equation will be

$$k_s \frac{\partial^2 T_s(x,t)}{\partial x^2} - C_s \frac{\partial T_s(x,t)}{\partial t} + E^2 \sigma_s(T_s) = 0$$

or

$$\frac{\partial^2 T_s(x,t)}{\partial x^2} - \frac{1}{K_s} \frac{\partial T_s(x,t)}{\partial t} + E^2 \frac{\sigma_s(T_s)}{K_s} = 0 \qquad 4.2$$

for $|x| \leq \frac{L_s}{2}$,

and

$$\frac{\partial^2 T_d(x,t)}{\partial x^2} - \frac{1}{K_d} \frac{\partial T_d(x,t)}{\partial t}, = 0 \qquad 4.3$$

for $|x| \geq \frac{L_s}{2}$,

where $K_s \triangleq \frac{K_s}{C_s}$ and $K_d \triangleq \frac{K_d}{C_d}$.

T_s and T_d are the temperatures of the semiconducting layer and its electrodes respectively above that of the heat sink substrate.

4.2.2 Boundary and Initial Conditions

Equations 4.2 and 4.3 are time-dependent, second-order partial, differential equations. It takes two initial conditions and four boundary conditions to determine the six integral constants. The first two initial conditions will be $T_s(x) = 0$ and $T_d(x) = 0$ at $t=0$; that is, before applying a bias voltage, the temperature is everywhere the same as that of the bath. The four boundary conditions required will be: (1) $\frac{\partial T_s}{\partial x} = 0$ at $x=0$

for all time t. The highest temperature will be assumed at the central plane where $x=0$. (2) The second boundary condition imposed is that $T_s(x,t)$ be continuous for all time t across the contact plane between the layer and electrodes. This is because if $T_s(x,t)$ is not continuous, then there would be an infinite heat sink existing in the contact plane. This is impossible. (3) The third boundary condition is that $\frac{\partial T_s(x,t)}{\partial x}$ must be continuous for all time t across the contact plane. This is because if $T_s(x,t)$ was not continuous, there would be an infinite energy source existing on the contact plane as in condition (2); this is impossible. (4) The final condition imposed is that the system's temperature drops to the bath temperature T_o at $|x| = L_s/2 + \epsilon$ where ϵ is a small positive quantity which can be as small as one wishes. That is, the temperature of the system goes down to T_o in the electrodes just over the junction plane.

Equation 4.2 and 4.3 are nonlinear, time-dependent, second-order, partial differential equations because of the nonlinear dependence of electrical conductivity on temperature. There will be no exact analytical solutions for these equations[23].

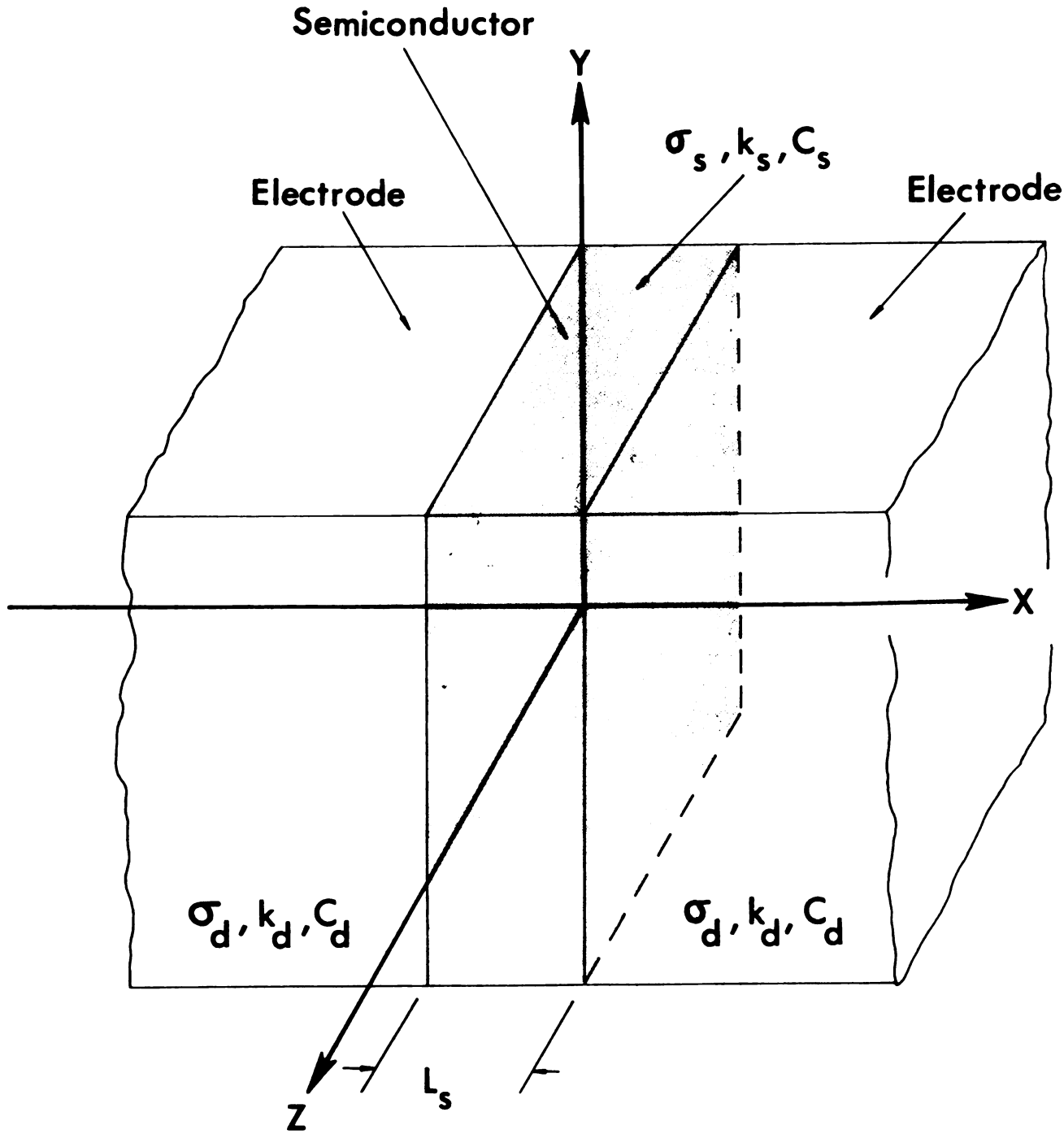

Figure 4. 2. The sandwich configuration under investigation.

If instead, one assumes that $\sigma(T)$ is field independent and can be expanded into Taylor series around ambient temperature T_o, to the first approximation, one will have

$$\sigma(T) = \sigma(T_o) + \sigma_T(T_o)(T-T_o), \qquad 4.4$$

where

$$\partial_T(T_o) = \frac{\partial\sigma}{\partial T}\Big|_{T=T_o}.$$

This kind of linearization of the electrical conductivity $\sigma(T)$ is justified by the fact that the electrical conductivity of the semiconducting layer investigated is relatively weakly temperature dependent around room temperature. In addition, one is only interested in the thermal behavior of the system near ambient temperature T_o, the above treatment will give us sufficient information. If higher order terms are needed, than a computer analysis would be required in order to solve the nonlinear, differential equations.

Now after substituting Equation 4.4 into Equations 4.2 and 4.3, a set of two ordinary second order time dependent partial differential equations, as shown below, is ready to be solved:

$$\frac{\partial^2 T_s(x,t)}{\partial x^2} - \frac{1}{K_s}\frac{\partial T_s(x,t)}{\partial t} + B_s T_s(x,t) = -A_s \qquad 4.5$$

for $|x| \leq \frac{L_s}{2}$,

and
$$\frac{\partial^2 T_d(x,t)}{\partial x^2} - \frac{1}{K_d} \frac{\partial T_d(x,t)}{\partial t} = 0, \qquad 4.6$$

for $|x| \geq \frac{L_s}{2}$,

where
$$B_s - \frac{E^2 \sigma_T(T_o)}{K_s} , \quad A_s = \frac{E^2 \sigma(T_o)}{K_s} \qquad 4.6$$

Note that this method of approaching the problem is different from that by Böer and Döhler[24]. Instead of a series expansion of electrical conductivity $\sigma(T)$ into temperature T, they expanded temperature function $T_s(x,t)$ into $T_s(x,t) = \sum_{\lambda} \sum_{\beta} e^{-i\lambda x} e^{\beta t}$, and solved the eigen equations. Their method proves to be tedious and lengthy, and the assumptions they make are buried in the analysis in such a manner that it is difficult at times to determine the conditions under which the analysis is valid.

4.2.3 Derivation and Results

By taking the Laplace transform of Equation 4.5 and 4.6, and by inserting the initial conditions, one obtains for $|x| \leq \frac{L_s}{2}$

$$\frac{\partial^2 V_s(x,p)}{\partial x^2} - (\frac{p}{K_s} - B_s) V_s(x,p) = - \frac{A_s}{p}, \qquad 4.7$$

and for $|x| \geq \frac{L_s}{2}$

$$\frac{\partial^2 V_d(x,p)}{\partial x^2} - \left(\frac{P}{K_d}\right) V_d(x,p) = 0, \qquad 4.8$$

where

$$V_s(x,p) \triangleq \int_o^\infty T_s(x,t)\, e^{-pt} dt \qquad 4.9$$

and

$$V_d(x,p) \triangleq \int_o^\infty T_d(x,t)\, e^{-pt} dt; \qquad 4.10$$

p is some positive number such that the above integrals converge.

From Equations 4.7 and 4.8,

for $|x| \leq \frac{L_s}{2}$

$$V_s(x,p) = \alpha(p) e^{q_s x} + \beta(p) e^{-q_s x} + \frac{A_s}{pq_s^2}, \qquad 4.11$$

and for $|x| \geq \frac{L_s}{2}$

$$V_d(x,p) = D(p) e^{-q_d\left(x - \frac{L_s}{2}\right)} + E(p) e^{q_d\left(x - \frac{L_s}{2}\right)}, \qquad 4.12$$

where $q_s^2 = \frac{P - K_s B_s}{K_s}$, $q_d^2 = \frac{P}{K_d}$ and $\alpha(p)$, $\beta(p)$, $D(p)$, $E(p)$ are all constants to be determined by invoking the boundary conditions.

From boundary condition (1), one has

$$\alpha(p) = \beta(p) \qquad 4.13$$

From condition (2) and Equation 4.13, one has

$$2\ \alpha(p) \cosh q_s \frac{L_s}{2} + \frac{A_s}{pq_s^2} = D(p) + E(p) \qquad 4.14$$

From condition (3), one has

$$2q_s\alpha(p)\ \sinh q_s \frac{L_s}{2} = -q_s[D(p) - E(p)] \qquad 4.15$$

From condition (4), one has

$$D(p)e^{-q_d\epsilon} + E(p)e^{q_d t} = 0 \qquad 4.16$$

Now, from Equation 4.16,

$$E(p) = -D(p)e^{-2q_d\epsilon},$$

and from Equation 4.15,

$$D(p) = \frac{-2q_s\alpha(p)\ \sinh q_s \frac{L_s}{2}}{q_d(1 + e^{-2q_d\epsilon})} \qquad 4.17$$

Substituting $D(p)$, $E(p)$ into 4.14, one obtains

$$\alpha(p) = \frac{-A_s\ q_d}{2\ pq_s^2\left[q_d \cosh q_s \frac{L_s}{2} + q_s \sinh q_s \frac{L_s}{2}\left(\frac{1-e^{-2q_d t}}{1+e^{-2q_d t}}\right)\right]} \qquad 4.18$$

Putting Equation 4.14 into 4.11 yields

$$V_s(x,p) = \frac{A_s}{pq_s^2}\ \left[1 - q_d \cosh q_s \frac{L_s}{2} + q_s \sinh q_s \frac{L_s}{2}\left(\frac{1-e^{-2q_d\epsilon}}{1+e^{-2q_d\epsilon}}\right)\right] \qquad 4.19$$

The corresponding time dependent temperature distribution function $T_s(x,t)$ will be

$$T_s(x,t) = \frac{1}{2\pi i}\int_{\alpha-i\infty}^{\alpha+i\infty} V_s(x,p)e^{pt}dp \qquad 4.20$$

where α should be chosen so that no poles of $V_s(x,p)$

be to the right half plane. By taking the integral along a closed path with radius R going to infinity, and with the aid of complex variable integration technique, it is easy to show that

$$T_s(x,t) = \sum_n \lim_{\substack{p\to p_n \\ \epsilon\to 0}} [(p-p_n)e^{pt}V_s(x,p)] \qquad 4.21$$

where p_n is the pole of $V_s(x,p)$.

Due to the difficulties in finding the poles of V_s in Equation 4.19, it will be wise to take the limit first in Equation 4.19 as $\epsilon \to 0$ before the inverse transform of $V_s(p,x)$ is taken. Doing this, one obtains

$$\lim_{\epsilon\to 0} V_s(x,p) = \lim_{\epsilon\to 0} \frac{A_s}{pq_s^2}\left[1 - \frac{q_d \cosh q_s x}{q_d \cosh q_s \frac{L_s}{2} + q_s \sinh q_s \frac{L_s}{2}\left(\frac{1-e^{-2q_d\epsilon}}{1+e^{-2q_d\epsilon}}\right)}\right]$$

$$= \frac{A_s}{pq_s^2}\left[1 - \frac{\cosh q_s x}{\cosh q_s \frac{L_s}{2}}\right] \qquad 4.22$$

After taking inverse Laplace transform of the above equation (see Appendix B), one obtains the desired time dependent, temperature distribution function $T_s(x,t)$ inside of the semiconducting layer as

$$T_s(x,t) = \frac{\sigma(T_o)}{\sigma_T(T_o)} \{ \sum_{n=1}^{\infty} \frac{1}{\frac{L_s^2}{4\pi}[\frac{E^2\sigma_T(T_o)}{K_s} - \frac{(2n-1)^2\pi^2}{L_s^2}]}$$

$$[(-1)^{n-1}(2n-1)e^{\frac{K_s}{C_s}(\frac{E^2\sigma_T(T_o)}{K_s} - \frac{(2n-1)^2\pi^2}{L_s^2})t}$$

$$- (-1)^{n-1}(2n-1)] \cos \frac{(2n-1)\pi x}{L_s}$$

$$- \frac{4}{\pi} \sum_{n=1}^{\infty} \frac{(-1)^n}{2n-1} e^{\frac{K_s}{C_s}[\frac{E^2\sigma_T(T_o)}{K_s} - \frac{(2n-1)^2\pi^2}{L_s^2}]t}$$

$$\cos \frac{(2n-1)\pi x}{L_s} - 1\} \qquad 4.23$$

4.2.4 Discussion

The time dependent temperature function at $x=0$ for various bias voltages is sketched in Figure 4.3. It is obvious that the temperature inside of the oxidized layer T_s, will increase without bound with time if

$$\frac{E^2\sigma_T(T_o)}{k_s} - \frac{(2n-1)^2\pi^2}{L_s^2} \geq 0, \qquad 4.24$$

where n is a positive integer.

If one takes $n=1$, the predominate term, one sees that if the electrical field E is higher than

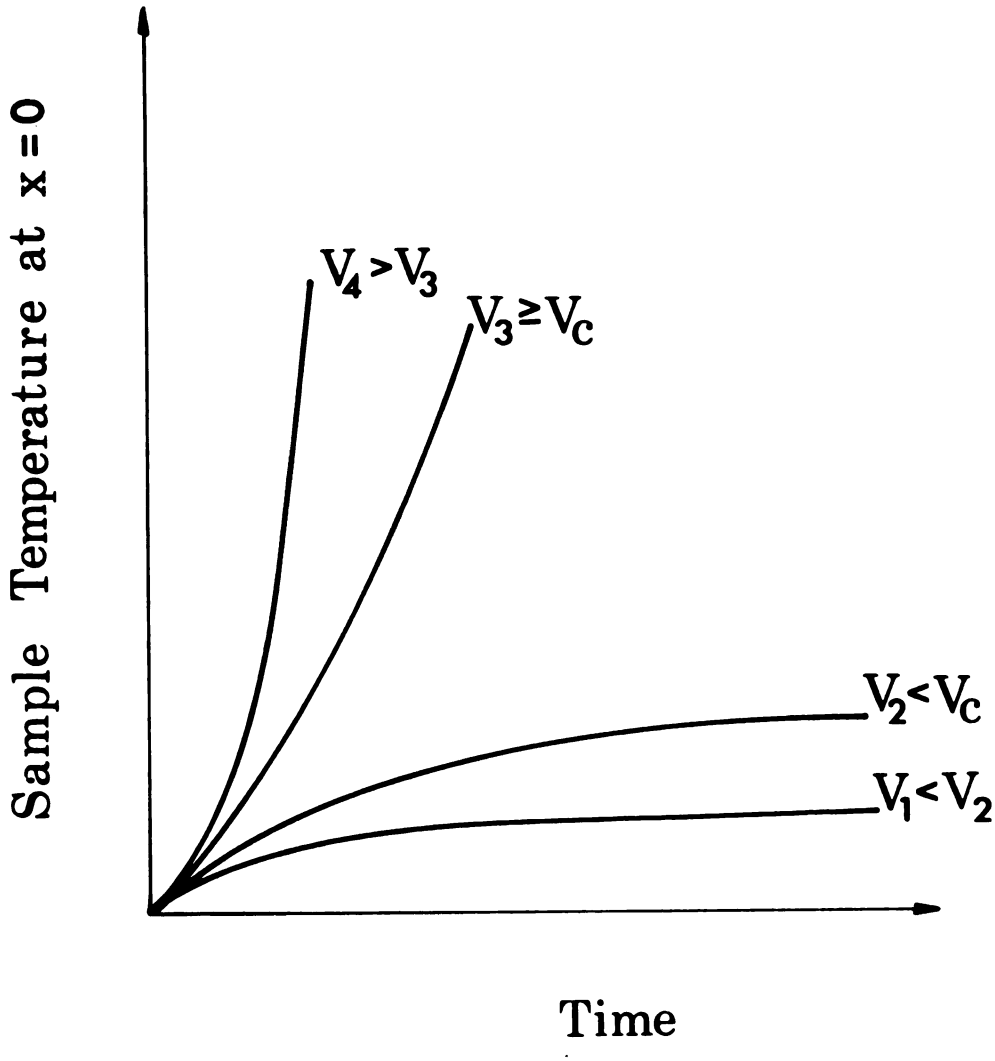

Figure 4. 3. Illustration of the sample's temperature at x = 0 as a function of time for various bias voltages.

$\frac{\pi}{L_s}\sqrt{\frac{K_s}{\sigma_T(T_o)}}$, the whole system will have a thermal instability such that electric switching will occur. On the other hand, if E is lower than $\frac{\pi}{L_s}\sqrt{\frac{K_s}{\sigma_T(T_o)}}$, temperature T_s in the layer will be stable and bounded; no switching effects will be expected to be observed. The desired threshold voltage required for the device to switch at ambient temperature T_o will thus be

$$V_c = L_s E_c = \pi\sqrt{\frac{K_s}{\sigma_T(T_o)}} \quad . \tag{4.25}$$

The threshold voltage is related quite simple to the thermal conductivity k_s and the rate of change of electrical conductivity with temperature. The higher the thermal conductivity k_s is, the higher the threshold voltage V_c required. This is because the heat generated inside of the layer will be conducted away more quickly if k_s is higher. Therefore, for the unit to have thermal instability and in order for switching to be initiated, the bias voltage should be high enough to generate sufficient Joule heat to overcome those conducted away to the bath.

From the expression for V_c given in Equation 4.25, one observes that the threshold voltage V_c will be affected by the bath temperature T_o since $\sigma_T(T_o)$ is dependent upon the bath temperature. For the amorphous semiconductors of interest, $\sigma_T(T_o)$ is a strictly increasing function of T_o in the vicinity of room temperature; therefore, V_c will decrease as ambient temperature T_o is raised. This is consistent with what other workers have observed[3-4].

The temperature dependence of electrical conductivity of the samples investigated was shown in Figure 3.1. Based upon this electrical conductivity data and Equation 4.25, it is natural to expect that the required threshold voltage V_c for the sample decreases with increasing bath temperatures. Figures 3.7 shows measured thermal dependence of the threshold voltages at various bath temperatures. It is obvious that they are qualitatively in agreement with the theory.

From Equation 4.25, V_c at T_o', T_o'', will be

$$V_c(T_o') = \pi\sqrt{\frac{k}{\sigma_T(T_o')}} \qquad 4.26$$

and $$V_c(T_o") = \pi\sqrt{\frac{k}{\sigma_T(T_o")}} \qquad 4.27$$

respectively.

Also from Equation 3.1, it is easy to show that

$$\frac{\sigma_T(T_o')}{\sigma_T(T_o")} = \exp.\ \frac{-4(T_o' - T_o")}{100} \qquad 4.28$$

Thus

$$\frac{V_c(T_o")}{V_c(T_o')} = \sqrt{\frac{\sigma_T(T_o')}{\sigma_T(T_o")}} = \exp.\ \frac{-2(T_o"-T_o')}{100}\ . \qquad 4.29$$

Figure 4.4 depicts the calculated thermal dependence of the threshold voltage V_c from Equation 4.29, in the temperature range from 300°K to 440°K for the case T_o' = 300°K. For comparison, the normalized threshold voltage observed in experiments was also shown. One concludes that basically the results are consistent with the theory.

The rise time of the temperature inside of the oxidized layer will be, from Equation 4.23,

$$T = \frac{1}{\frac{k_s}{c_s}\left(\frac{E^2\sigma_T(T_o)}{k_s} - \frac{\pi^2}{L_s^2}\right)} \qquad 4.30$$

for n=1. This is not exactly the switching delay time but is in proportional to it.

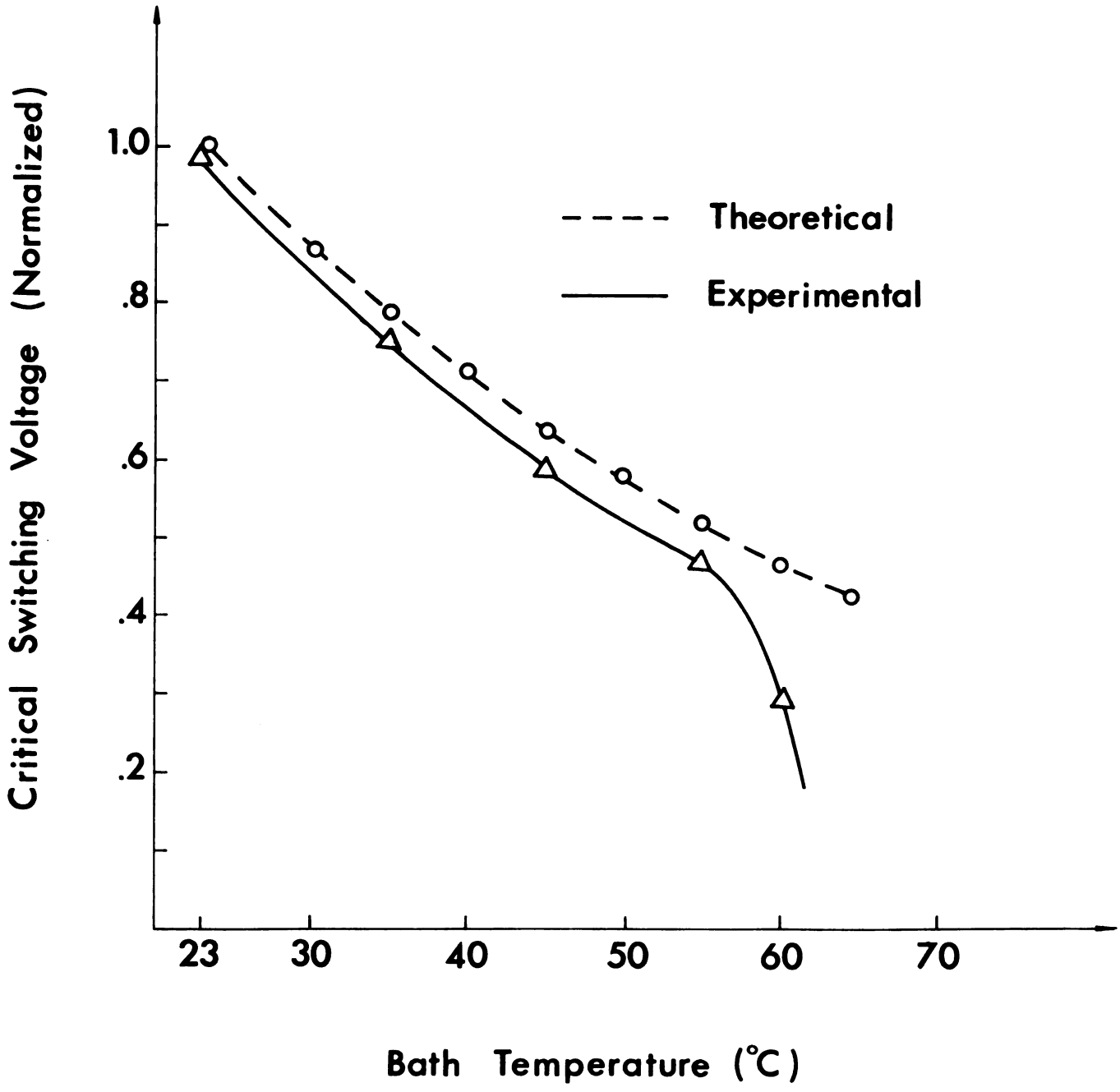

Figure 4.4. Critical voltage required to actuate switching for various bath temperatures. (At 23° C, the switching voltage was 4.2V.)

From this expression, it is evident that the switching delay time T_d will be affected by both the applied bias voltage and the bath temperature in the following manner: An incremental rise in the applied voltage will cause an incremental decrease in the time required for thermal runaway to be initiated. This is because the rise in applied voltage causes an incremental rise in the instantaneous power being dissipated in the sample; consequently, the temperature of the sample will rise more quickly and thermal runaway will be initiated earlier.

An incremental rise in $\sigma_T(T_o)$ will also result in an incremental decrease in the time required for thermal runaway to be initiated. This is due to the fact that less Joule heating is required to raise the sample's conductivity an incremental amount; consequently, if the bias voltage is held constant, the time required for switching to be initiated is decreased.

Figure 3.8 shows the observed time delay of the unit for various bias voltages. From the oscilloscope, traces it is obvious that as the

bias voltage increases, T_d decreases. Figure 3.9 illustrates how the time delay of the unit is affected by the bath temperature. Once again it is obvious that all experimental data supports the above theory.

More specifically, one can express Equation 4.30 in the following manner:

$$T_d = \frac{L_s^2 C_s / \sigma_T(T_o)}{V^2 - V_c^2} \qquad 4.31$$

where $V_c^2 \equiv \frac{\pi^2 k_s}{\sigma_T(T_o)}$ is the threshold voltage required at bath temperature T_o. The delay time T_1, T_2 corresponding to bias voltage V_1, V_2 at the same bath temperature T_o will then be

$$T_1 = \frac{L_s^2 C_s / \sigma_T(T_o)}{V_1^2 - V_c^2} \qquad 4.32$$

$$T_2 = \frac{L_s^2 C_s / \sigma_T(T_o)}{V_2^2 - V_c^2} \qquad 4.33$$

respectively. Thus

$$\frac{T_1}{T_2} = \frac{V_2^2 - V_c^2}{V_1^2 - V_c^2} \qquad 4.34$$

Equation 4.34 expresses the normalized delay time for various bias voltages at ambient temperature T_o.

For the case observed, T_o is 300°K, V_c is approximately 4 volts. Equation 4.34 is depicted in Figure 4.5. Also shown is the normalized delay time vs. bias voltage data observed in the series of pictures in Figure 3.8. From these two curves in Figure 4.5, it is obvious that basic agreements exists between theory and experiments.

While considering a completely different material and using a completely different analytic approach Böer and Ovshinsky[9] obtained a very similar expression for the threshold voltage V_c. They expanded the sample's temperature $T_s(x,t)$ into Fourier series summations which were in terms of x and t, and then substituted T_s into the governing thermal transport equation. After solving the obtained eigen equation from thermal equation and taking approximation, the desired expression for threshold voltage V_c was then derived yielding[9]

$$V_c = \pi(\sigma_{oo}\beta/k_s)\frac{1}{2}, \qquad 4.35$$

where k_s is thermal conductivity, $\sigma_{oo}\beta$ is $\frac{\partial\sigma(T)}{\partial T}$ at temperature T_o, and σ, the electrical conductivity of the materials they investigated was

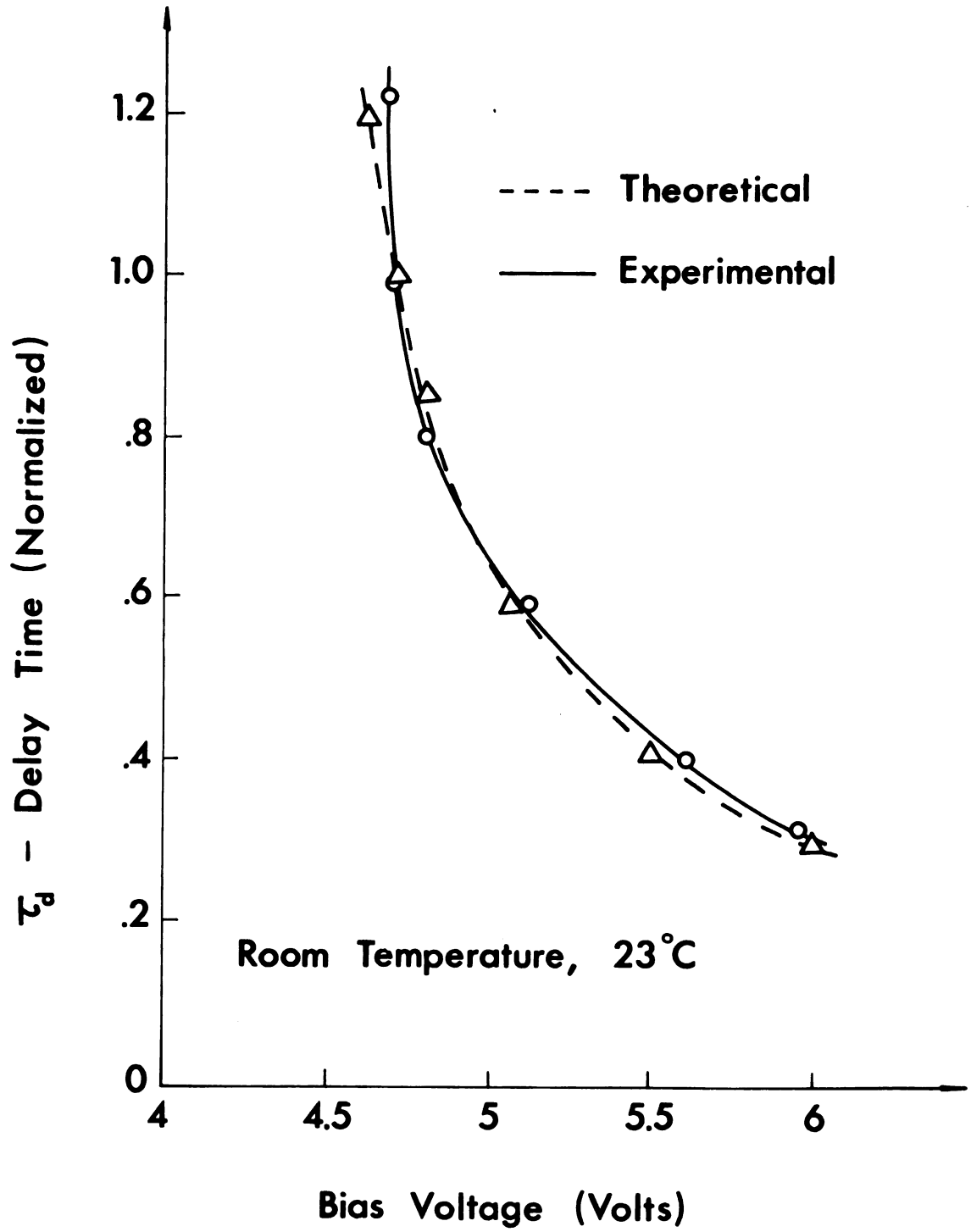

Figure 4.5. Switching delay time as a function of applied voltage for a typical oxidized vanadium foil. (For a 4.7V bias, the measured delay time was 10 μ sec.)

$$\sigma(T) = \sigma_{oo} \exp \beta(T-T_o) \qquad 4.36$$

Their approach proves to be much more lengthy and tedious. Also, assumptions were buried in the middle of their analysis, making it difficult to follow and to understand implications of these simplifications. All of our assumptions were made at the very beginning, making it easy to follow and gain physical insight of the meaning and implications of the assumptions. Furthermore, our approach lends itself much more readily to computer analysis.

The discrepancy between theory and experiments in Figure 4.4 is due to the fact that higher order terms in the Taylor expansion of $\sigma(T)$ were neglected. The radical derivation for temperature above 55°C is because, above this temperature, the assumption stated in Equation 4.4 is not valid.

All data and theoretical curves presented here have been normalized because of the uncertainty at the present time in the absolute values of k_s, σ_s and C_s. This uncertainty exists because the

samples investigated were not composed of a single, well defined vanadium-oxygen complex but rather of an assortment of complexes.

Despite this uncertainty in the absolute value of k_s and C_s, the experimental evidence presented suggests that preswitching behavior of the oxidized vanadium foil is strongly dependent upon the thermal properties of the materials.

4.3 Temperature Distribution and Threshold Voltage of the VO_2 Film--Planar Configuration

4.3.1 Introduction

The second sample geometry of interest was first employed by Berglund and Walden[3] in their study of thin-film inductance effects (See Figure 4.6). Our motives for studying this configuration are three fold: (1) To show how easily the techniques and approximations made in the analysis of the first configuration can be extended to explain the important features of this new structure. (2) To derive an expression for the threshold voltage for this second configuration and compare it with the experimental observations of Berglund and Walden[3].

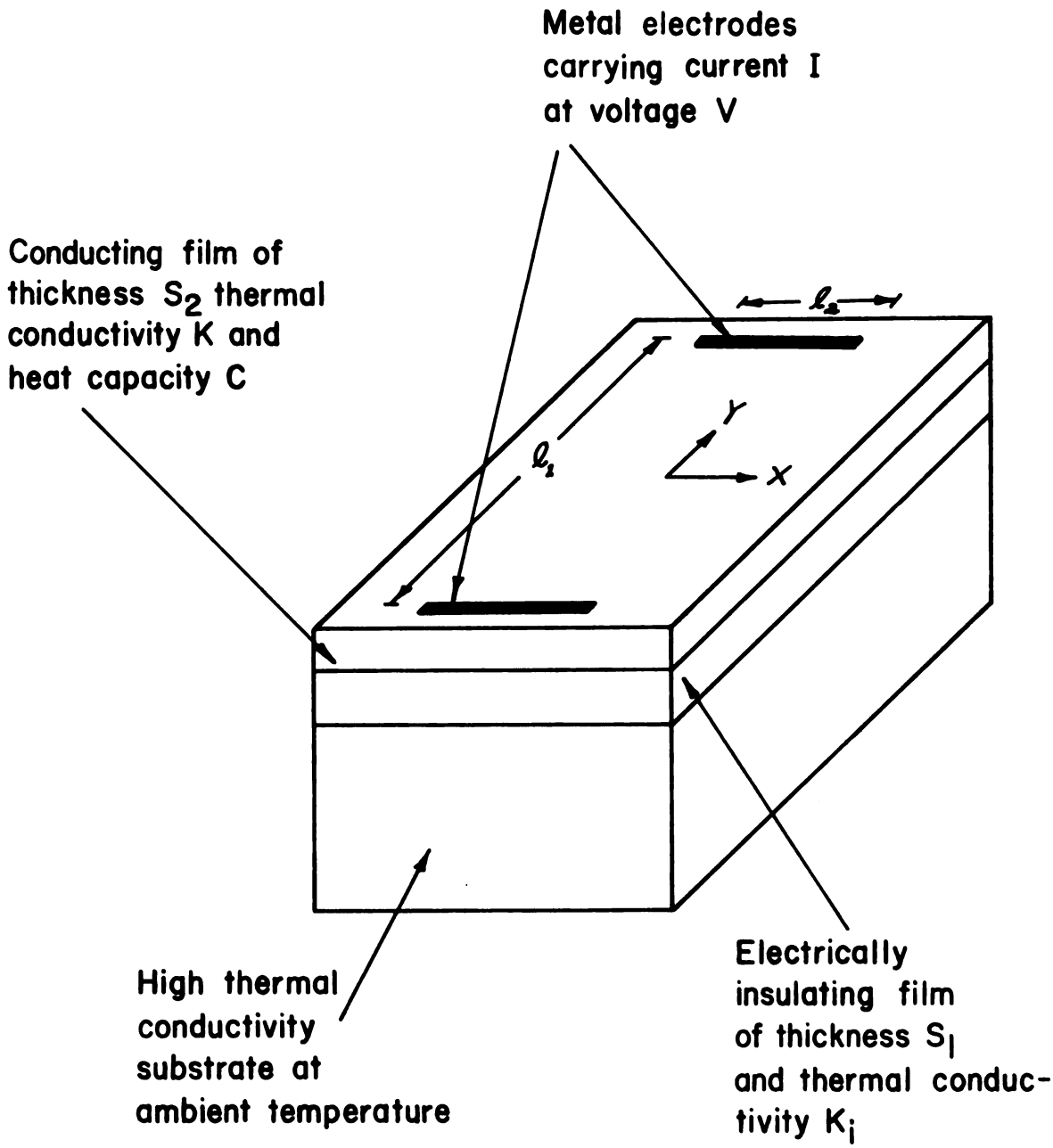

Figure 4.6. Illustration of the thin-film, planax configuration to be analyzed.

(3) To compare these two thermal boundary configurations in order to determine which possesses the most desirable switching properties.

4.3.2 Geometry and Assumptions

The structure of interest is a conducting vanadium dioxide (VO_2) thin film of thickness S_2, thermal conductivity k and volume specific heat capacitance C, placed on a thin electrically insulating film of thickness S_1 and thermal conductivity k_i. This insulator film in turn resides on a substrate of high thermal conductivity which acts as a thermal heat sink. Two parallel electrodes of spacing ℓ_1 and length ℓ_2 are deposited onto the electrically conducting film as shown in Figure 4.6. Vanadium dioxide under consideration has a phase transition at 68°C accomplished by a discontinuous change in resistivity of a factor of the order of 10^4 from the high-resistance to low-resistance to low-resistance state.

Since the switching and inductance properties of VO_2 are a direct consequence of the material's thermal properties, the nonohmic behavior observed in the preswitching, low-conductance

state could be predicted by solving the thermal transport equation, subjected to the proper boundary conditions.

For simplicity, the following assumptions are made. (1). There is neglible heat flow through the electrical contacts.

(2). There is no temperature gradient in the plane perpendicular to the film surface.

(3). There is no lateral heat flow in the insulating film.

(4). The thermal conductivity of the substrate is much higher than any others, so that the insulator-substrate interface can be assumed to always remain at the ambient temperature T_o'.

(5). Only conduction of heat is concerned, heat convection or radiation will not be considered.

(6). The thin film under consideration is assumed to be homogeneous and isotopic; therefore, the electric field in the thin-film layer is uniform.

(7). All the parameters k_i, k, C are all assumed to be temperature, electric field and spatially independent.

4.3.3 Derivation and Results

The rate that energy is delivered to a unit volume of the thin film active layer by the conduction electrons will be $E^2\sigma(T)$, where E is the strength of the externally applied electric field and $\sigma(T)$ is electrical conductivity of the thin-film active layer. The rate that energy is stored in a unit volume of the active layer is $C\frac{\partial T}{\partial t}$. The rate at which energy is conducted away through the SiO_2 to the heat-sink substrate will be $\frac{k_i T}{S_1 S_2}$, and finally the rate that energy diffuses laterally out of a unit volume of the active layer will be $k\frac{\partial^2 T}{\partial x^2}$. Thus, from the conservation of energy, the heat flow equation will be

$$\frac{\partial^2 T(x,t)}{\partial x^2} - \frac{k_i T(x,t)}{k S_1 S_2} - \frac{C}{k}\frac{\partial T(x,t)}{\partial t} + \frac{E^2 \partial(T)}{k} = 0 \qquad 4.37$$

where $T(x,t)$ is the temperature of the conducting film above that of the heat sink substrate.

Due to the nonlinearity of the thermal dependence of electrical conductivity, no exact solution can be obtained for this nonlinear partial differential equation.

By utilizing the same approach developed in Section 4.2.2, one can simplify Equation 4.37 and solve it subject to the appropriate initial conditions and thermal boundary conditions, thereby obtaining an explict expression for $T(x,t)$ in terms of the bulk properties of the material, the dimensions of the structure and the applied electric field strength. The principal assumptions made in the course of the analysis are that $\partial(T) = \partial_o + (\frac{\partial\sigma}{\partial T})T$ and that the electric field is applied as a step function at time $t=o$. Equation 4.37 can then be rewritten as follows:

$$\frac{\partial^2 T_1}{\partial x^2} - \frac{1}{K_1}\frac{\partial T_1}{\partial t} + B_1 T_1 = -A \qquad 4.38$$

for $|x| \leq \frac{l_2}{2}$, and

$$\frac{\partial^2 T_2}{\partial x^2} - \frac{1}{K_2}\frac{\partial T_2}{\partial t} + B_2 T_2 = 0 \qquad 4.39$$

for $|x| \geq \frac{l_2}{2}$, where

$$K_1 = \frac{k_1}{C_1} = K_2 = \frac{k_2}{C_2}, \qquad 4.40$$

$$B_1 = (\frac{E^2\frac{\partial\sigma}{\partial T}}{k} - \frac{k_i}{kS_1S_2}), \qquad 4.41$$

$$B_2 = \frac{-k_i}{kS_1S_2} \qquad 4.42$$

and $$A = \frac{E^2\sigma_o}{k}.$$

In order to determine the constants of integration, the initial conditions and boundary conditions must be specified. Since the external electric field is assumed to be a step function applied at time $t=0$, the initial temperature of the thin film will be equal to bath temperature and furthermore $T_1(x,0) = T_2(x,0) = 0$.

The four boundary conditions specified are as follows: (1). T is continuous across the interface $|x| = \frac{\ell_2}{2}$, otherwise $\frac{\partial T}{\partial x}$ would be unbounded, and an infinite heat sink should reside at the boundary.

(2). $\frac{\partial T}{\partial x}$ is continuous across the interface $|x| = \frac{\ell_2}{2}$, otherwise an infinite heat source would exist at the boundary.

(3). Due to symmetry, $\frac{\partial T}{\partial x} = 0$ at $x=0$ for all time t.

(4). T remains bounded as x approaches infinity.

By taking the Laplace transform, and with the aid of the initial conditions, Equations 4.38 and 4.39 now become

$$\frac{\alpha^2 V_1(x,p)}{\alpha x^2} - \left(\frac{P}{K_1} - B_1\right)V_1 = -\frac{A}{P} \qquad 4.44$$

for $|x| \leq \frac{\ell_2}{2}$ and

$$\frac{\alpha^2 V_2(x,p)}{\alpha x^2} - \left(\frac{P}{K_2} - B_2\right)V_2 = 0 \qquad 4.45$$

for $|x| \geq \frac{\ell_2}{2}$, where

$$V_1(p,x) = \int_0^\infty T_1(x,t)\exp(-pt)dt, \qquad 4.46$$

$$V_2(p,x) = \int_0^\infty T_2(x,t)\exp(-pt)dt, \qquad 4.47$$

and p is some positive number such that the above integrals converge.

Letting $q_1^2 = \frac{P-K_1B_1}{K_1}$, $q_2^2 = \frac{P-K_2B_2}{K_2}$ and then solving Equations 4.44 and 4.45, one obtains

$$V_1(p,x) = G_1(p)e^{q,x} + G_2(p)e^{-q,x} + \frac{A}{Pq_1^2}, \qquad 4.48$$

and

$$V_2(p,x) = G_3(p)e^{q_2(x - \frac{\ell_2}{2})} + G_4(p)e^{q_2(x + \frac{\ell_2}{2})} \qquad 4.49$$

where G_1, G_2, G_3, G_4 are constants of integration.

From boundary condition (1), $G_1=G_2$. From boundary condition (4), $G_4=0$. From boundary conditions (2) and (3),

$$G_1(p) = \frac{A}{2}\frac{q_2}{Pq_1^2}\quad\frac{1}{q_2\cosh q_1\frac{\ell_2}{2} + q_1\sinh q_1\frac{\ell_2}{2}}.$$

Thus one obtains

$$V_1(p,x) = \frac{A}{Pq_1^2}\left[1 - \frac{q_2 \cosh q_1 x}{q_2 \cosh q_1 \frac{\ell_2}{2} + q_1 \sinh q_1 \frac{\ell_2}{2}}\right] \qquad 4.50$$

For convenience, three cases of the above equation will be discussed separately.

CASE A ----- $q_1 = q_2 = q$

This means that $B_1 = B_2 = B$. Equation 4.50 then reduces to

$$V_1(p,x) = \frac{A}{Pq^2}\left[1 - \frac{1}{2}e^{-q(\frac{\ell_2}{2} - x)} - \frac{1}{2}e^{q(\frac{\ell_2}{2} + x)}\right], \qquad 4.51$$

where $|x| \leq \frac{\ell_2}{2}$.

Letting $(p-KB) = p'$, $\sqrt{\frac{P'}{K}} = q'$. $V_1(p,x)$ becomes

$$V_1(p,x) = \frac{A}{B}\left\{\frac{1}{P'}\left[1 - \frac{1}{2}e^{-q'(\frac{\ell_2}{2} - x)} - \frac{1}{2}e^{-q'(\frac{\ell_2}{2} + x)}\right]\right.$$
$$\left. - \left[\left(\frac{1}{P'+KB}\right)\left(1 - \frac{1}{2}e^{-q'(\frac{\ell_2}{2} - x)} - \frac{1}{2}e^{-q'(\frac{\ell_2}{2} + x)}\right)\right]\right\} \qquad 4.52$$

With the assistance of an inverse Laplace transform table, one can show that the corresponding temperature function $T_1(x,t)$ in time domain will be[27]

$$T_1(x,t) = -\frac{A_1}{B} + \frac{A_1}{B} e^{KBt}\left[1 - \frac{1}{2}\operatorname{erfc}\frac{(\frac{\ell_2}{2}-x)}{2\sqrt{Kt}} - \frac{1}{2}\operatorname{erfc}\frac{\frac{\ell_2}{2}-x}{2\sqrt{Kt}}\right]$$

$$+ \frac{1}{4}\frac{A_1}{B}\left\{e^{-(\frac{\ell_2}{2}-x)\sqrt{-B}}\operatorname{erfc}\left[\frac{(\frac{\ell_2}{2}-x)}{2\sqrt{Kt}} - \sqrt{-KBt}\right]\right.$$

$$+ e^{-(\frac{\ell_2}{2}+x)\sqrt{-B}}\operatorname{erfc}\left[\frac{(\frac{\ell_2}{2}+x)}{2\sqrt{Kt}} - \sqrt{-KBt}\right]$$

$$+ e^{(\frac{\ell_2}{2}-x)\sqrt{-B}}\operatorname{erfc}\left[\frac{(\frac{\ell_2}{2}-x)}{2\sqrt{Kt}} + \sqrt{-KBt}\right]$$

$$+ e^{(\frac{\ell_2}{2}+x)\sqrt{-B}}\operatorname{erfc}\left[\frac{(\frac{\ell_2}{2}+x)}{2\sqrt{Kt}} + \sqrt{-KBt}\right]$$

for $|x| \leq \frac{\ell_2}{2}$.

From Equation 4.53, $T_1(x,t)$ will be unstable only if $B = (-\frac{k_i}{kS_1S_2}) > 0$. As a consequence of the assumption $q_1 = q_2 = q$, $E^2 \frac{\partial\sigma(T)}{\partial T}$ or E will be zero and $B_1 = B_2 = -\frac{k_i}{kS_1S_2}$, will be smaller than zero. This is the trivial case since no electrical field is applied to the thin film. Also from Equation 4.53, it is obvious that the final temperature T_f for $B < 0$ will be

$$T_f = \lim_{\substack{B<0 \\ t\to\infty}} T_1(x,t) = 0. \qquad 4.54$$

This is what one expects. No thermal instability occurs in this case.

CASE B ----- $q_1 > q_2$.

Physically this has no meaning since if $q_1 > q_2$,

$$\{P - K(\frac{E^2 \frac{\partial\sigma}{\partial T}}{k} - \frac{k_i}{kS_1S_2})\} > \{P + K \frac{k_i}{kS_1S_2}\},$$

or $E^2 \frac{\partial\sigma}{\partial T} < 0$. For the substance discussed, $\frac{\partial\sigma}{\partial T}$ is always larger than zero in the temperature range interested. Thus, this case will not be considered further.

CASE C ----- $q_1 < q_2$.

For this case, $E^2 \frac{\partial\sigma}{\partial T} > 0$, which is the situation of most interest to us. With the aid of the convolution theorem, one will be able to find the inverse Laplace transform of $V_1(p,x)$ in Equation 4.50. Since the primary concern of this section is to figure out the threshold voltage for which the system will possess a thermal instability, it is convenient to discuss the problem in frequency (or p) domain instead of the time domain. This is because the corresponding time-dependent, temperature-distribution function obtained from Equation 4.50 will be too involved to be discussed here. In order to be better prepared to discuss the results of this analysis, the following definitions and theorem are introduced:

Definitions

(1). If $f(t)$ is classified as piecewise regular if in every interval of the form $0 \leq t_1 \leq t \leq t_2$, $f(t)$ is bounded and has at most a finite number of discontinuities.

(2). $f(t)$ is of exponential order if there exists constants α, M and T such that

$$e^{-\alpha t}|f(t)| < M \quad \text{for every} \quad t > T,$$

where the greatest lower bound α_o of the set $\{\alpha\}$ is called the abscissa of convergence of $f(t)$.

Theorem

If $f(t)$ and $f'(t)$ are both piecewise regular and of exponential order, and if the abscissa of convergence of $f'(t)$ is negative, then

$$\lim_{p \to 0} p\, L[f(t)] = \lim_{t \to 0} f(t),$$

provided that these limts exist[27].

In realistic applications of this theorem, $L[f(t)]$ will be known. Hence it is desirable that conditions be expressed in terms of $L[f(t)]$ rather than $f(t)$. This can be done, since it is possible to show that the above theorem can be applied if there is any value of p with nonnegative real part for which $p\, L[f(t)]$ is unbounded but can be applied if no such value exists.

Now, from Equation 4.50,

$$pV_1(p,x) = \frac{A}{P-KB_1} \frac{\sqrt{P-KB_2}\cosh\sqrt{P-KB_1}\,x}{\sqrt{P-KB_2}\cosh\sqrt{P-KB_1}\frac{\ell_2}{2} + \sqrt{P-KB_1}\sinh\sqrt{P-KB_1}\frac{\ell_2}{2}} \qquad 4.55$$

The poles of $pV_1(p,x)$ will be $P_1=KB_1$ and those for p for which

$$\tanh\sqrt{P-KB_1} = -\sqrt{\frac{P-KB_2}{P-KB_1}}$$

(Recall that $B_1 = \frac{E^2\frac{\partial\sigma}{\partial T} - \frac{k_i}{kS_1S_2}}{k}$, and $B_2 = -\frac{k_i}{kS_1S_2}$).

If the electric field E is smaller than $\sqrt{\frac{k_i}{S_1S_2\frac{\partial\sigma}{\partial T}}}$, it is easy to show that all the poles will lie in the left half plane. According to the above theorem, the device temperature T_f as time goes to infinity will be

$$\begin{aligned} T_f &= \lim_{t\to\infty} T_1(x,t) \\ &= \lim_{p\to 0} p\,V_1(p,x) \\ &= \frac{A}{|KB_1|} \frac{\sqrt{|KB_2|}\cosh\sqrt{|KB_1|}\,x}{\sqrt{|KB_2|}\left[\cosh\sqrt{|KB_1|}\frac{\ell_2}{2} + \sqrt{|KB_1|}\sinh\sqrt{|KB_1|}\frac{\ell_2}{2}\right.} \end{aligned} \qquad 4.56$$

If T_f falls below the phase transition temperature, where the electrical conductivity increases abruptly, there will be no thermal instability; this is because the temperature of the system will be always bounded and finite for all time.

On the contrary, if the electric field E is so high that $E^2 > \frac{k_i}{S_1 S_2 \frac{\partial \sigma}{\partial T}}$, then the system will be sure to have thermal instability and, therefore, electric switching will be initiated.

Due to the nonlinearity of the thermal dependence of electrical conductivity $\sigma(T)$, the final temperature T_f of the system, under the application of an electric field E, where $E < \sqrt{\frac{k_i}{S_1 S_2 \frac{\partial \sigma}{\partial T}}}$ will be higher than the value for T_f predicted by Equation 4.56. This is because of the assumption made neglecting higher order terms in the Taylor series expansion of $\sigma(T)$. Thus, the critical electric field $E_C = \sqrt{\frac{k_i}{S_1 S_2 \frac{\partial \sigma(T_o)}{\partial T}}}$ is not exactly the desired threshold field, it is a little higher than the desired value.

If the applied voltage falls below some threshold value, the system investigated will be eventually come to the state of virtual equilibrium; that is, $\frac{\partial T}{\partial t} = 0$, $\frac{\partial^2 T}{\partial x^2} = 0$. The equilibruim temperature T_{eq} will be, from Equation 4.38,

$$\frac{k_i}{S_1 S_2} T_{eq} = E^2 \partial(T). \qquad 4.57$$

The graphic solution of the above equation, as shown in Figure 4.7, gives two equilibrium temperatures of the system, T_α and T_β. If there is a thermal disturbance $T_1(x,t)$, which is due to thermal fluctuation, and where $T_1(x,t) \ll T_\alpha$, T_β, then only T_α will be the temperature at which the system will remain stable. The reason is follows:

Since $T_1(x,t)$ can always be expressed as the superposition of a series summation, $T_1(x,t) = \sum_{\lambda,\nu} e^{i\lambda x} e^{\nu t}$, from the small-signal theory, it is also true that $\sigma(T)$ can be approximated by

$$\sigma(T) = \sigma(T_{eq}) + \sigma_T(T_{eq}) T_1(x,t), \qquad 4.58$$

where $|T_1| \ll T_\alpha$, T_β. Substituting $\sigma(T)$ and $T_1(x,t)$ into the basic governing Equation 4.38, one will have

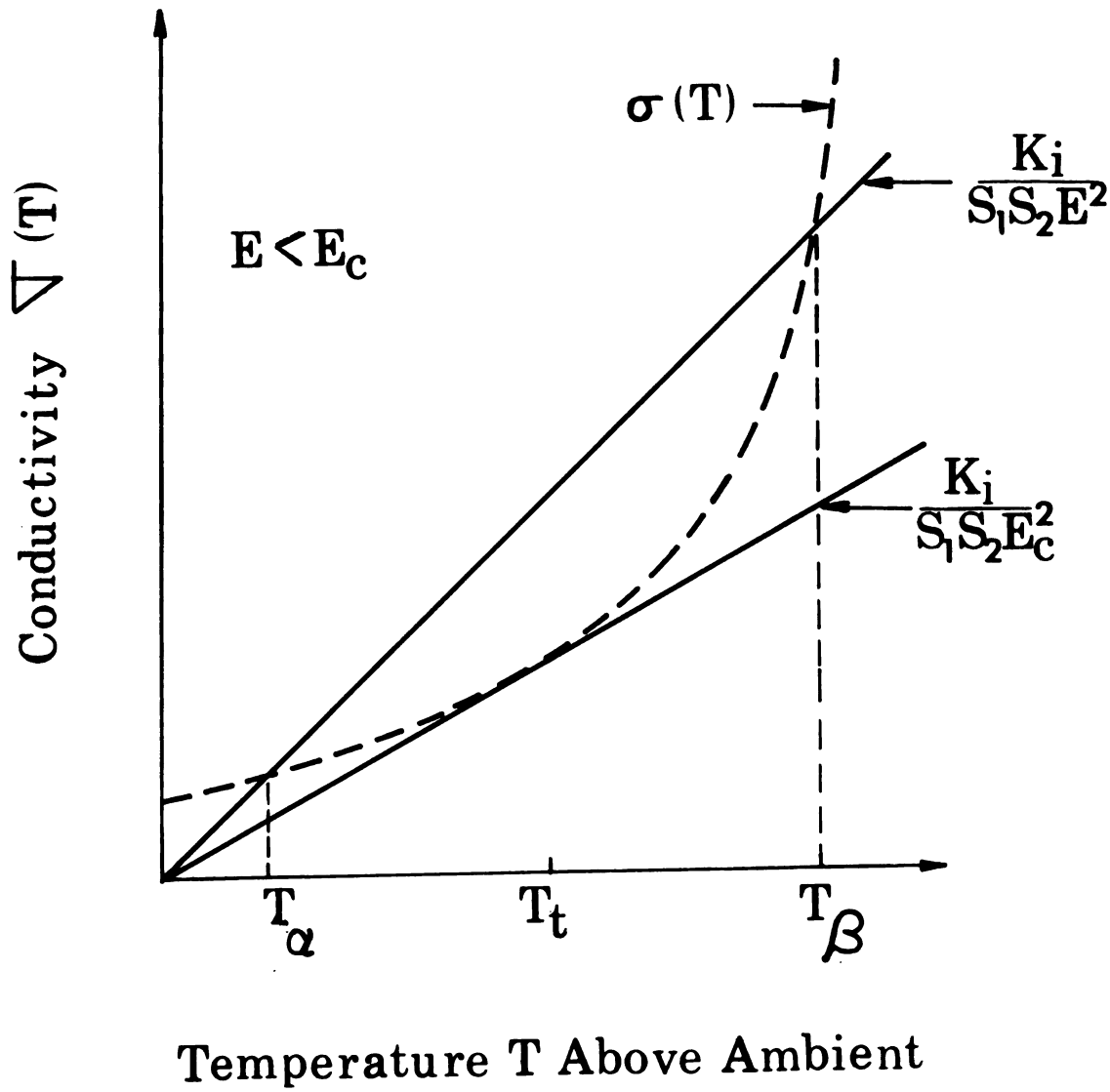

Figure 4. 7. Graphical solution of the time-independent temperature equation. T_α and T_β correspond to the equilibrium temperatures.

$$-\lambda^2 - \frac{\nu}{\frac{k}{C}} + \left(\frac{E^2\sigma_T(T_{eq})}{k} - \frac{k_i}{kS_1S_2}\right) = 0$$

or

$$\nu = \frac{1}{C}\left(E^2\sigma_T(T_{eq}) - \frac{k_i}{S_1S_2}\right) - \frac{k}{C}\lambda^2, \qquad 4.59$$

λ^2 is always positive since λ is real. Thus if

$$\left[E^2\sigma(T)(T_{eq}) - \frac{k_i}{S_1S_2}\right] \geq 0,$$

ν will be positive, and the temperature perturbation $T_1(x,t)$ will grow up as time goes on. At the equilibrium temperature T_β, $\sigma_T'(T_{eq})$ always larger than $\frac{k_i}{S_1S_2E^2}$. On the other hand, when the system is at equilibrium temperature T_α, where $\sigma_T(T_\alpha) < \frac{k_i}{S_1S_2E^2}$, the negative value of ν will cause the thermal perturbation $T_1(x,t)$ to decay. Thus the system will be restored to remain stable at equilibrium temperature T_α instead of T_β.

From the above discussion, it is concluded that in order for the system to reach the unstable equilibrium temperature T_β such that a phase transition may occur, the applied bias voltage V_C should be such that T_α coincides with T_β; that is, as can be seen in Figure 4.7, the bias field should be such that the heat dissipation line

$\frac{k_i}{S_1 S_2 E^2} T$ is tangent to the electrical conductivity curve $\sigma(T)$ at $T_\alpha = T_\beta$. The physical meaning of this is that the Joule heat $E^2\sigma(T_\alpha)$ generated exactly equals the heat dissipated $\frac{k_i}{S_1 S_2} T$. For lower electric fields, the temperature of the system will never go beyond T_α since the heat dissipated will exceed the heat supplied for the temperature $T > T_\alpha$.

It is now clear that the desired threshold voltage for this configuration to actuate the thermal instability and consequently initiate electric switching will be

$$V_C = \ell_1 \cdot E_C, \tag{4.60}$$

where E_C is such that functions $\frac{k_i}{S_1 S_2 E^2} T$ and $\sigma(T)$ have only one point of intersection.

More specifically,

$$V_C = \ell_1 E_C = \ell_1 \sqrt{\frac{k_i}{S_1 S_2 \sigma_T(T_t)}}, \tag{4.61}$$

where $\sigma_T(T_t)$ is the rate of change of electrical conductivity σ of the thin film investigated at T_t, where T_t is the tangent temperature of the

dissipation line $\frac{k_i}{S_1 S_2 E^2} T$ drawn from ambient temperature T_o to $\sigma(T)$. Through $\sigma_T(T_t(T_o))$, V_C is affected by the bath temperature T_o as has been observed in most of the cases.[3,4]

4.3.4 Discussion

Due to the manner in which the electrical conductivity $\sigma(T)$ of VO_2 depends upon temperature,[3] one would expect that the higher $\sigma_T(T_t(T_o))$ would be, the lower the threshold voltage V_C would be. This can be easily verified by the observing data of Berglund and Walden[3].

The temperature dependence of electrical conductivity of VO_2 film can be approximated by

$$\sigma(T) = 10^{[1.52(4 - \frac{100}{T}) - 1.74]}, \qquad 4.62$$

This σ-T relationship is sketched in Figure 4.8. From this Figure, $\frac{\partial\sigma[T_t(T_o)]}{\partial T}$ at various ambient temperatures T_o were estimated and are presented in Table III. From this data, the required threshold voltage was calculated using Equation 4.61 at various ambient temperatures T_o and the results are summarized in Table IV.

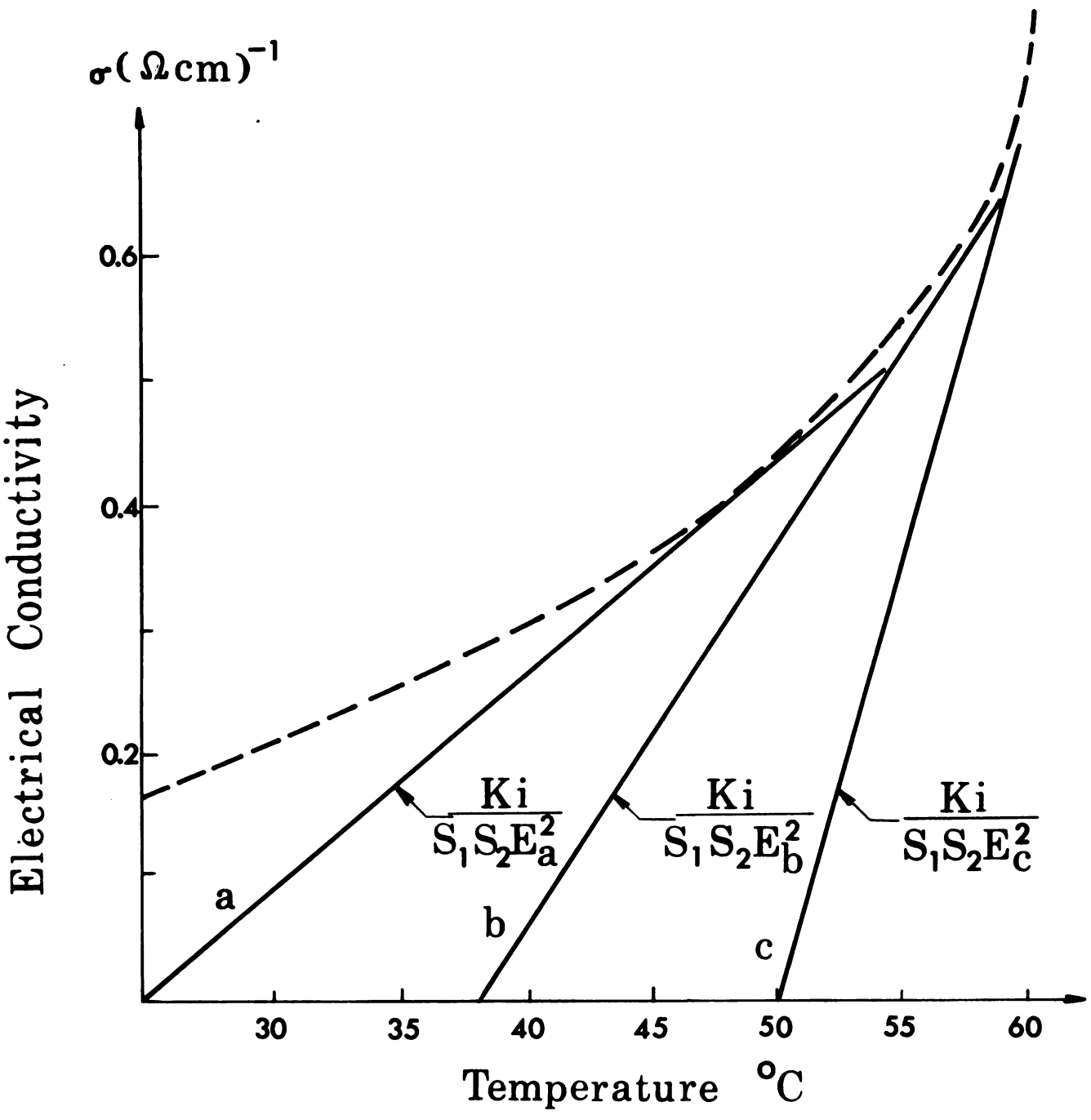

Figure 4. 8. Graphical solution of the threshold voltage required for the VO_2 layer to switch for bath temperaturs of (a) 25° C, (b) 38° C and (c) 50° C.

TABLE III

$\frac{\partial\sigma}{\partial T}(T_t(T_o))$ of VO_2 Thin Film At Various Ambient Temperatures

Ambient Temperature T_o(°C)	$\frac{\partial\sigma}{\partial T}(T_t(T_o))(\Omega_{cm})^{-1}$
25	.0167
30	.02
35	.024
38	.027
45	.04
50	.06
55	.10

TABLE IV

Threshold Voltage V_c at Various Ambient Temperatures

Ambient Temperature T_o(°C)	V_c(Volts)
25	93.5
30	67
35	61.3
38	57.5
45	47.4
50	38.6
55	28

In the above calculations the following values for sample geometry and bulk parameters were used:

$$k = 0.06\ W/cm°K,\ k_i = 0.010\ W/cm°K,\ \ell_1 = 30\mu m$$
$$S_1 = 10^{-4}cm.,\ S_2 = 10^{-5}cm.,\ C = 3.3J/cm^3°K.$$

The threshold voltages measured by Berglund and Walden[3] at bath temperature 25°C, 38°C, and 50°C were 57 volts, 52.5 volts and 35 volts respectively. Figure 4.9 shows the threshold voltages required for the VO_2 thin film to accuate electric switching at various ambient temperatures both by Equation 4.61 derived and experimental data measured. It is obvious that good agreement exists between the experiments and theory.

The discrepancy between theory and experiments comes from the insufficient information on the temperature dependence of electrical conductivity of VO_2 film employed by Berglund and Walden[3]. The estimated threshold voltage from the derived Equation 4.61 may thus be a little higher than the experimental data. Nevertheless, the theory confirms once again that the switching effect in VO_2 thin films has a thermal origin as predicted by other observers[3,16-17].

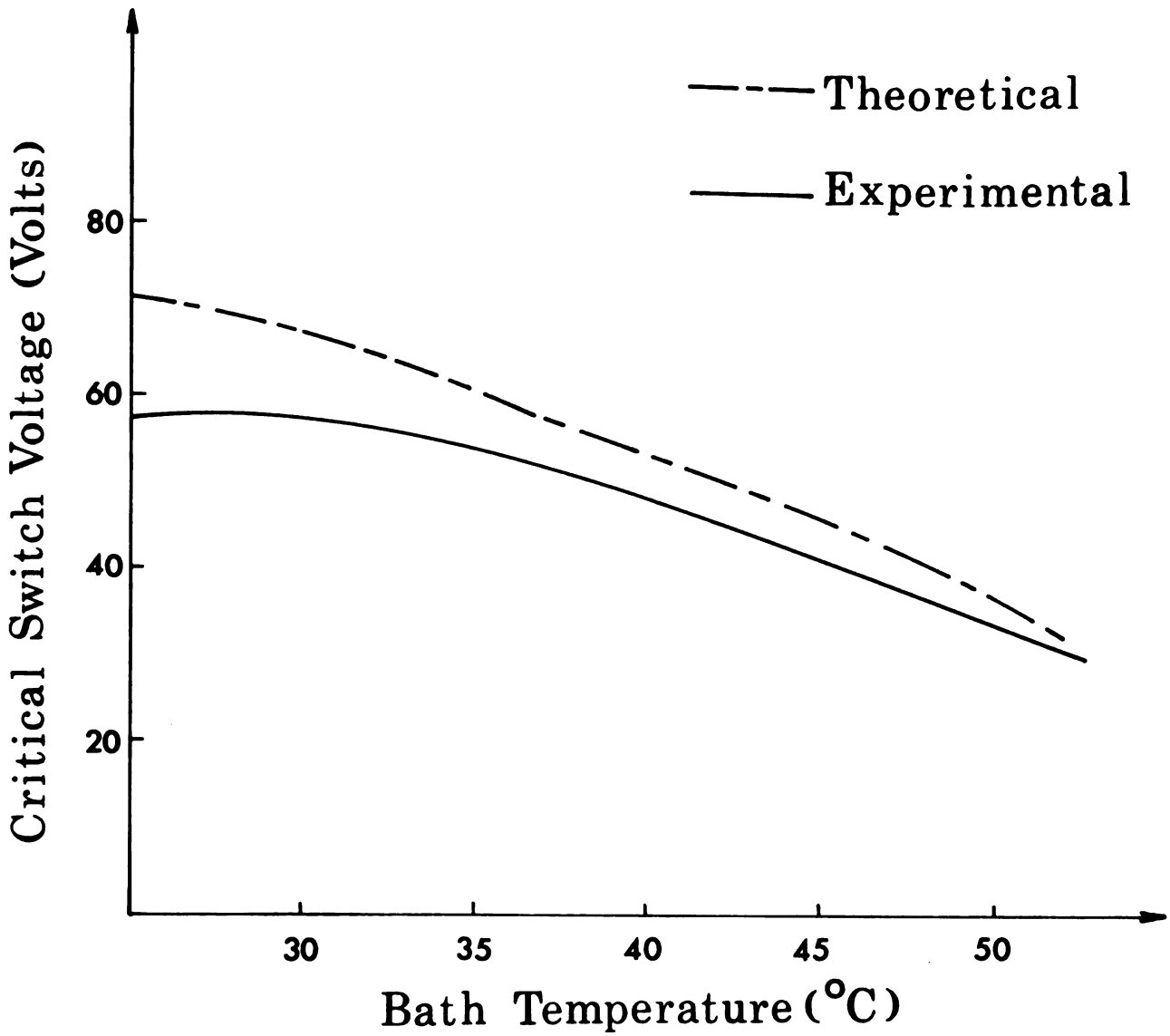

Figure 4.9. Voltage required to actuate switching for various bath temperatures.

4.4 Negative Resistance

4.4.1 Introduction

Various negative-differential-resistance effects in solids have been observed. Most of these effects are associated with junction or contact phenomena[11,25-26]. The most notable examples are the p-n-p-n junction devices and the tunnel diode. Other negative-differential-resistance effects may be classified as true, bulk properties of solids. For example, the Gunn effect is a voltage-controlled, switching phenomena which is due to an inherent instability associated with the nonlinear carrier mobility in certain solids. Current-controlled negative resistance, as found in many amorphous semiconductors and transition metal oxides, is associated with electrical breakdown which originates from a thermal initiated local instability.

By totally neglecting effects due to lattice temperature gradients, Ridley[11] has shown, using irreversible thermodynamics, that the current-controlled, negative-differential resistance in a bulk device favors the formation of thermal filaments,

providing a current fluctuation occurs. The negative differential resistance observed in an isothermal system has also discussed by Burgess[26].

Presented here is an alternative approach which assumes that a current filament is formed inside of a bulk material and then by neglecting the effects due to the transverse temperature gradient, a critena for observing current-controlled, negative-differential resistance in a bulk device is established and discussed. This method of approach is opposite to that done by Ridley[11] and is more general than the case discussed by Burgess[26]. In short, Ridley[11] discussed the adiabatic case, Burgess[26] discussed the isothermal non-adiabatic case, while what will be discussed here is the case of non-adiabatic non-isothermal conditions.

4.4.2 Derivation; Results and Discussion

The structure of interest is shown in Figure 4.6. It is a thin-film semiconductor of thickness S_2, thermal conductivity k and electrical conductivity $\sigma(T)$. $\sigma(T)$ is expressed by Equation 3.1. The layer is placed on an electrically insulating film of

thickness S_1 which possesses a thermal conductivity k_i. This insulator film in turn resides on a substrate of high thermal conductivity which acts as a thermal heat sink. By totally neglecting effects due to lattice temperature gradients, the energy balance equation (Equation 4.37) reduces to

$$E^2\sigma(T) = \frac{k_i}{S_1 S_2} T \qquad 4.63$$

in the steady state, where E is the applied electric field in the thin film.

Now take one unit volume element of the thin film for consideration. Suppose that there is a temperature perturbation due to thermal fluctuations such that part of the thin film with area a has a higher temperature T_a and the remaining part b which has temperature T_b.

Let σ_a, σ_{ao}, σ_b, σ_{bo} be the corresponding electric conductivity of the thin film at temperature T_a, T_{ao}, T_b, and T_{bo} respectively, and define

$$M_a \triangleq \lim_{T_a \to T_{ao}} \frac{\sigma_a - \sigma_{ao}}{T_a - T_{ao}} \qquad 4.64$$

and

$$M_b \triangleq \lim_{T_b \to T_{bo}} \frac{\sigma_b - \sigma_{bo}}{T_b - T_{bo}} . \qquad 4.65$$

Then

$$\sigma_a = \sigma_{ao} + M_a(T_a - T_{ao}) = \sigma_{oa}' + M_a T_a \qquad 4.66$$

and

$$\sigma_b = \sigma_{bo} + M_b(T_b - T_{bo}) = \sigma_{ob}' + M_b T_b, \qquad 4.67$$

where

$$\sigma_{oa}' \triangleq \sigma_{oa} - M_a T_{oa} \qquad 4.68$$

$$\sigma_{ob}' \triangleq \sigma_{ob} - M_b T_{ob}. \qquad 4.69$$

From Equation 4.63, one has

$$\sigma_a = \sigma_{oa}' + M_a T_a = \frac{k_i}{S_1 S_2 E^2} T_a \qquad 4.70$$

$$\sigma_b = \sigma_{ob}' + M_b T_b = \frac{k_i}{S_1 S_2 E^2} T_b \qquad 4.71$$

Thus

$$T_a = \frac{-\sigma_{oa}'}{M_a\left(1 - \dfrac{k_i}{S_1 S_2 E^2 M_a}\right)}, \qquad 4.72$$

and

$$T_b = \frac{-\sigma_{ob}'}{M_b\left(1 - \dfrac{k_i}{S_1 S_2 E^2 M_b}\right)}. \qquad 4.73$$

From the current density expression

$$J = E\sigma = E(a\sigma_a + b\sigma_b) = E_a(\sigma_{oa}' + M_a T_a) + E_b(\sigma_{ob} + M_b T_b)$$
$$= J_a + J_b, \qquad 4.74$$

it is obvious that J is function of both E and T; therefore,

$$\frac{dJ(E,t)}{dE} = \frac{dJ_a}{dE} + \frac{dJ_b}{dE}$$

$$= \frac{\partial J_a}{\partial E}\Big|_{T_a} + \frac{\partial J_b}{\partial E}\Big|_{T_b} + \left(\frac{\partial J_a}{\partial T_a}\right)\Big|_E \frac{dT_a}{dE} + \left(\frac{\partial J_b}{\partial T_b}\right)\Big|_E \frac{dT_b}{dE}, \qquad 4.75$$

where

$$\frac{\partial J}{\partial E}\Big|_T = a\sigma_a + b\sigma_b = a\sigma_{oa}' + b\sigma_{ob}' + aM_aT_a + bM_bT_b,$$

$$\frac{\partial J_a}{\partial T_a}\Big|_E = aEM_a,$$

and

$$\frac{\partial J_b}{\partial T_b}\Big|_E = bEM_b,$$

these relationships can be obtained from Equation 4.74, and

$$\frac{dT_a}{dE} = 2\,\frac{\sigma_{oa}'}{M_a}\left(1 - \frac{k_i}{S_1S_2M_aE^2}\right)^{-2} \frac{k_i}{S_1S_2M_a}\,E^{-3} \qquad 4.76$$

and

$$\frac{dT_b}{dE} = 2\,\frac{\sigma_{ob}'}{M_b}\left(1 - \frac{k_i}{S_1S_2M_bE^2}\right)^{-2} \frac{k_i}{S_1S_2M_b}\,E^{-3} \qquad 4.77$$

can be obtained from Equations 4.72 and 4.73. Substituting the above Equations into Equation 4.75, one obtains an expression for $\frac{dJ}{dE}$:

$$\frac{dJ}{dE} = a\sigma_{oa'} + b\sigma_{ob'} + aM_aT_a + bM_bT_b$$

$$+ 2a\sigma_{oa'}\left(1 - \frac{k_i}{S_1S_2E^2M_a}\right)^{-2} \frac{k_i}{S_1S_2M_2} E^{-2}$$

$$+ 2b\sigma_{ob'}\left(1 - \frac{k_i}{S_1S_2E^2M_b}\right)^{-2} \frac{k_i}{S_1S_2M_b} E^{-2} \qquad 4.78$$

Equation 4.78 can further be simplified to yield (Appendix C)

$$\frac{dJ}{dE} = a\sigma_a\left[1 + \frac{2M_aT_a}{\sigma_{oa'}}\right] + b\sigma_b\left[1 + \frac{2M_bT_b}{\sigma_{ob'}}\right] \qquad 4.79$$

For negative resistance to be observed, one requires

$$\frac{dJ}{dE} < 0;$$

that is

$$\left(\frac{a}{b}\right)\left(\frac{\sigma_a}{\sigma_b}\right)\left(\frac{1 + 2\frac{M_aT_a}{\sigma_{oa'}}}{1 + 2\frac{M_bT_b}{\sigma_{ob'}}}\right) < -1$$

or

$$\left(\frac{a}{b}\right)\left(\frac{\sigma_a}{\sigma_b}\right)\left(\frac{2 - \frac{M_aT_a}{\sigma_{oa'}} - 1}{2\frac{M_bT_b}{\sigma_{ob'}} + 1}\right) > 1. \qquad 4.80$$

For convenience, the electrical conductivity $\sigma(T)$ is divided into two parts by the temperature T_t, where T_t is the tangent temperature of the dissipation line $\frac{k_i}{S_1S_2E^2}T$ drawn from the ambient

temperature to the $\sigma(T)$ vs. T curve. These two parts may be represented as follows:

$$M(T) < \frac{k_i}{S_1 S_2 E^2} \quad \text{for} \quad T < T_t \tag{4.81}$$

and

$$M(T) > \frac{k_i}{S_1 S_2 E^2} \quad \text{for} \quad T > T_t \tag{4.82}$$

where $M(T) = \frac{\partial \sigma(T)}{\partial T}\Big|_T$.

The following conclusions may then be drawn from Equations 4.79 and 4.80.

(1) If the thermal fluctuation occurs when temperature of the unit is below T_t, then from 4.79, $\frac{\alpha J}{\alpha E} > 0$ for all $T < T_t$, since $\sigma_{oa'}$, $\sigma_{ob'}$, M_a and M_b are all positive. Therefore, no negative-differential resistance will be observed. Physically, this is because, for sample temperatures below T_t, the rate that the electrical conductivity increases with temperature is so low that in order to meet and overcome the heat conducted away to the bath, it is required that a higher electric field be applied. Since the only method of increasing the temperature of the unit is to raise the electric field, no thermal runaway condition exists.

(2) Consider the case where the thermal fluctuation occurs at the time the unit temperature just stabilizes at T_t. For this case

$$m_a = m_b,$$

and

$$\sigma_{oa'} = \sigma_{ob'} = 0.$$

From Equation 4.78,

$$dJ = a\ m\ T_a + b\ m\ T_b > 0. \qquad 4.83$$

This implies that the negative-differential resistance will not be observed even if the temperature of the unit reaches the characteristic temperature T_t. For vanadium dioxide, this characteristic temperature is the phase transition temperature. Thus it is concluded that the switching action observed in VO_2 thin films does not start at the time when the unit temperature uniformly reaches T_t.

(3) Consider the case where the temperature of the device is uniform; i.e. $b \to 0$ and $a \to 1$. For this case, no thermal fluctuation exists within the material; consequently, from Equation 4.79,

$$\frac{dJ}{dE} = a\sigma_a \left[1 + \frac{2M_a T_a}{\sigma_{oa'}}\right] \qquad 4.84$$

In order for the negative differential resistance to be observed, one requires that

$$\frac{dJ}{dE} < 0.$$

Thus $(M_a T_{oa} - \sigma_{oa}) > 0$,

and hence

$$M_a > \frac{\sigma_{oa}}{T_{oa}} .$$

Therefore, for this isothermal case, the switching action starts at the moment the temperature of the unit reaches T_t.

(4) From the least entropy production rate principle, the existing negative-differential resistance favors the formation of a current channel. From conclusion (3), it is obvious that even if no current channel forms, the negative-differential resistance may be observed. Thus one concludes that negative-differential resistance is not a necessary condition for formation of a current channel, and vice versa. From Equation 4.80, one observes that the greater the rate of change of electrical conductivity with temperature in the region of thermal filament a, the higher the possibility of observing the negative-differential resistance. Usually area a is much smaller than area b and that in order for negative-differential resistance to be observed,

the temperature in channel a must be high enough so that the ratios $\frac{\sigma_a}{\sigma_b}$ and $(\frac{M_a T_a}{|\sigma_{oa}'|})/(\frac{M_b T_b}{|\sigma_{ob}'|})$ are much larger than one. Therefore, even after the formation of a thermal filament, if the channel is too small, the negative-differential resistance might still not be observable.

4.5 Negative Resistance for the Isothermal, Steady-State Case.

After sectionwise linearization of any temperature dependence of electrical conductivity curve $\sigma(T)$, (see Figure 4.10) one defines the following regions R_i $(i = 1,2,3,\ldots,n)$ as

$T_1 \leq T \leq T_2$ as R_1

$T_2 \leq T \leq T_3$ as R_2

$T_i \leq T \leq T_{i+1}$ as R_i

$T_n \leq T \leq T_{n+1}$ as R_n.

Then the electrical conductivity at temperature T within Region R_i can be approximated by

$$\sigma(T) = \sigma_{oi} + m_i(T-T_i) \qquad 4.85$$

where

$$\sigma_{oi} = \sigma_{o1} + \sum_{i=1}^{i-1} (T_{i+1}-T_i)m_i, \qquad 4.86$$

$$m_i = \lim_{T_{i+1} \to T_i} \frac{\sigma(T_{i+1}) - \sigma(T_i)}{T_{i+1} - T_i} \qquad 4.87$$

and σ_{o1} is the electrical conductivity at temperature T_1, σ_{oi} is that at T_i. For convenience, T_1, the bath temperature which all the device temperatures referred to, is set to zero.

For the steady-state, isothermal situation, the thermal transport equation (Equation 4.37) reduces to

$$E^2\sigma(T) = \frac{k_i T}{S_1 S_2} \qquad 4.88$$

Thus, the voltage $V(T)$ across the device is given simply by

$$V^2(T) = E^2 \ell_1^2 = \frac{k_i \ell_1 T}{S_1 S_2 \sigma(T)} \qquad 4.89$$

or alternately by

$$V^2(T) = \frac{k_i \ell_1^2 T}{S_1 S_2 M_i (T-T_i)+\sigma_{oi}} \qquad 4.90$$

for region R_i.

Applying Ohm's law in region R_i, one obtains the following expression for the current $I(T)$ in the film:

$$I(T) = V(T)\sigma(T)\ \frac{\ell_2 S_2}{\ell_1}\ , \qquad 4.91$$

where $(\ell_2 S_2)$ is the cross-sectional area of the unit investigated. One has for region R_i,

$$I^2(T) = \left(\frac{S_2 \ell_2^2 k_i}{S_1}\right) T \left[M_i(T-T_{i-1}) + \sigma_{oi}\right]. \qquad 4.92$$

From Equation 4.92,

$$T = \frac{T_{oi}}{2} \pm \left[\frac{|T_{oi}|}{2}\left(1 + 4\,\frac{I^2(T)}{I_{oi}^2}\right)^{1/2}\right] \qquad 4.93$$

where

$$T_{oi} \equiv \left(\frac{M_i T_i - \sigma_{oi}}{M_i}\right) \qquad 4.94$$

$$I_{oi}^2 \equiv \frac{S_2 L_2^2 k_i (M_i T_i - \sigma_{oi})^2}{M_i S_1} \qquad 4.95$$

Note here that T_{oi} may be positive or negative depending upon where it is in the region. In addition, since the temperature of interest is always above that of the bath temperature, the negative sign in Equation 4.93 should be discarded.

Substituting Equation 4.93 into Equation 4.89, one obtains

$$V^2(T) = V_{oi}^2 \; \frac{T_{oi}/2 + \frac{|T_{oi}|}{2}\left[1 + 4\,\frac{I^2(T)}{I_{oi}^2}\right]^{1/2}}{-\frac{T_{oi}}{2} + \frac{|T_{oi}|}{2}\left[1 + 4\,\frac{I^2(T)}{I_{oi}^2}\right]^{1/2}} \qquad 4.96$$

where

$$V_{oi} \equiv \sqrt{\frac{\ell_1^2 k_i}{S_1 S_2 M_i}} \qquad 4.97$$

Several cases must be discussed:

Case 1 $(T_{oi} < 0)$

This means that if the device temperature T reaches region R_i and the temperature dependent electrical conductivity $\sigma(T)$ is as indicated by branch 1, then $M_i < \frac{\sigma_{oi}}{T_i}$, that is, the slope of the straight line from origin to point (T_i, σ_{oi}).

For this case, Equation 4.96 becomes

$$V^2(T) = \frac{k_i L_1^2}{S_1 S_2 M_i} \frac{-1 + \left[1 + 4 \frac{I^2(T)}{I_{oi}^2}\right]^{1/2}}{1 + \left[1 + 4 \frac{I^2(T)}{I_{oi}^2}\right]^{1/2}}$$

$$= \frac{k_i L_1^2}{S_1 S_2 M_i} \frac{\left[\left(1+4 \frac{I^2}{I_{oi}^2}\right)^{1/2} - 1\right]^2}{4 \frac{I^2}{I_{oi}^2}} \qquad 4.98$$

Therefore,

$$V(I) = \sqrt{\frac{k_i L_1^2}{S_1 S_2 M_i}} \frac{\left[\left(1+4 \frac{I^2}{I_{oi}^2}\right)^{1/2} - 1\right]}{2 \left|\frac{I}{I_{oi}}\right|} \qquad 4.99$$

and

$$I(V) = \frac{-|I_{oi}|}{V_{oi}} \frac{V}{\left(\frac{V^2}{V_{oi}^2} - 1\right)} \qquad 4.100$$

Thus

$$\frac{\partial I}{\partial V} = \left(\frac{|I_{oi}|}{V_{oi}}\right)\left(\frac{V^2}{V_{oi}^2} - 1\right)^{-2}\left(\frac{V^2}{V_{oi}^2} + 1\right) > 0 \qquad 4.101$$

while

$$\frac{\partial^2 I}{\partial V^2} = -2\left(\frac{|I_{oi}|}{V_{oi}}\right)\left(\frac{V^2}{V_{oi}^2} - 1\right)^{-3}\frac{V}{V_{oi}}\left(\frac{V^2}{V_{oi}} + 3\right) > 0 \qquad 4.102$$

since from Equation 4.96, $V < V_{oi}$ for $T_{oi} < 0$.

Case 2 ($T_{oi} > 0$)

This means that if the device temperature T reaches region R_i and the temperature dependent electrical conductivity $\sigma(T)$ is as indicated by branch 2, then $M_i > \frac{\sigma_{oi}}{T_1}$; that is, the slope of electrical conductivity m_i is greater than the slope of the straight line from origin to the point (T_i, σ_{oi}).

For the case, from Equation 4.96, $V > V_{oi}$, and one observes that I-V relation is

$$I(V) = \frac{|I_{oi}|}{V_{oi}}\, V \left(\frac{V^2}{V_{oi}^2} - 1\right)^{-1}. \qquad 4.103$$

Thus

$$\frac{\partial I}{\partial V} = -\left(\frac{|I_{oi}|}{V_{oi}}\right)\left(\frac{V^2}{V_{oi}^2} - 1\right)^{-2}\left(\frac{V^2}{V_{oi}^2} + 1\right) < 0, \qquad 4.104$$

and

$$\frac{\partial^2 I}{\partial V^2} = 2\left(\frac{|I_{oi}|}{V_{oi}}\right)\left(\frac{V^2}{V_{oi}^2} - 1\right)^{-3} \frac{V}{V_{oi}^2}\left(\frac{V^2}{V_{oi}^2} + 3\right) > 0. \qquad 4.105$$

Case 3 $\left(m_i = \frac{\sigma_{oi}}{T_i}\right)$

This is the case the slope of the electrical conductivity m_i is equal to that of the straight line drawn from origin to the point (T_i, σ_{oi}). From Equation 4.96, $V = V_{oi}$, thus $\frac{\partial I}{\partial V} \to \infty$ as can be seen from Equation 4.103.

Case 4 $(m_i = 0)$

This is the case when the device electrical conductivity is the temperature independent. From Equation 4.88, one sees the linear relationship between voltage V and current I.

Case 5 $(m_i \to \infty)$

In this case an abrupt change in the electrical conductivity is observed as in some metals or oxides at their melting points or phase transition temperature. From Equation 4.103, one has

$$I(V) = \lim_{m_i \to \infty} \frac{|I_{oi}|}{V} V V_{oi}^2 (V^2 - V_{oi}^2)^{-1}$$

$$= \lim_{m_i \to \infty} S_2 |M_i T_i - \sigma_{oi}| V \cdot \left(\frac{\ell_1^2 k_i}{S_1 S_2 M_i}\right)\left(V^2 - \frac{\ell_1^2 k_i}{S_1 S_2 M_i}\right)^{-1}$$

$$= \lim_{m_i \to \infty} |T_i - \frac{\sigma_{oi}}{M_i}| \left(\frac{\ell_1^2 k_i}{S_1}\right) \frac{V}{\left(V^2 - \frac{\ell_1^2 k_i}{S_1 S_2 M_i}\right)}$$

$$= T_i \frac{\ell_1^2 k_i}{S_1} \frac{1}{V} . \qquad 4.106$$

Thus

$$\frac{\partial I}{\partial V} = T_i \frac{\ell_1^2 k_i}{S_1} \frac{-1}{V^2} < 0. \qquad 4.107$$

The following conclusions are drawn:

1. For the negative differential resistance to be observed, the given $\sigma(T)$ vs. T curve should be intersected at least twice by the straight line $\frac{k_i T}{S_1 S_2 E^2}$ drawn from the origin. More specifically, positive differential resistance can only be observed if the temperature of the unit is below T_t.

2. In any section of the I-V characteristic curve, the curvature is always nonnegative, that is, the I-V curve is always concave up, or, $\frac{d^2 I}{dV^2} \geq 0$.

3. Any abrupt increase in electrical conductivity with temperature can result in the appearance of negative differential resistance.

Figure 4.10 illustrates a typical electrical conductivity versus temperature relationship which is exhibited by VO_2 and other semiconductors which undergo phase transitions. The corresponding I-V characteristic curve predicted in the steady-state isothermal case for such a material is also depicted in Figure 4.11.

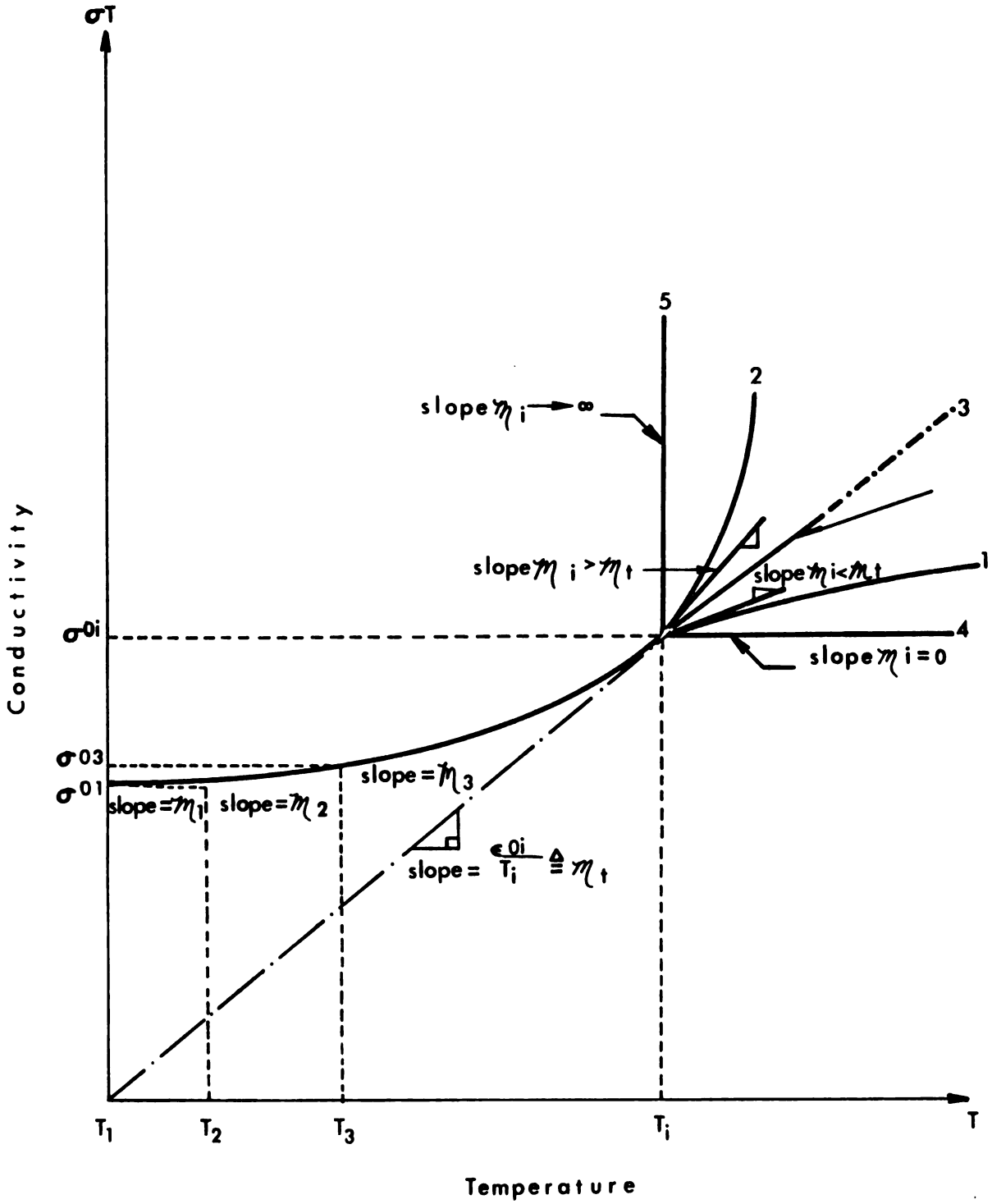

Figure 4. 10. Illustration of the section-wise linearization of a typical sample's electrical conductivity.

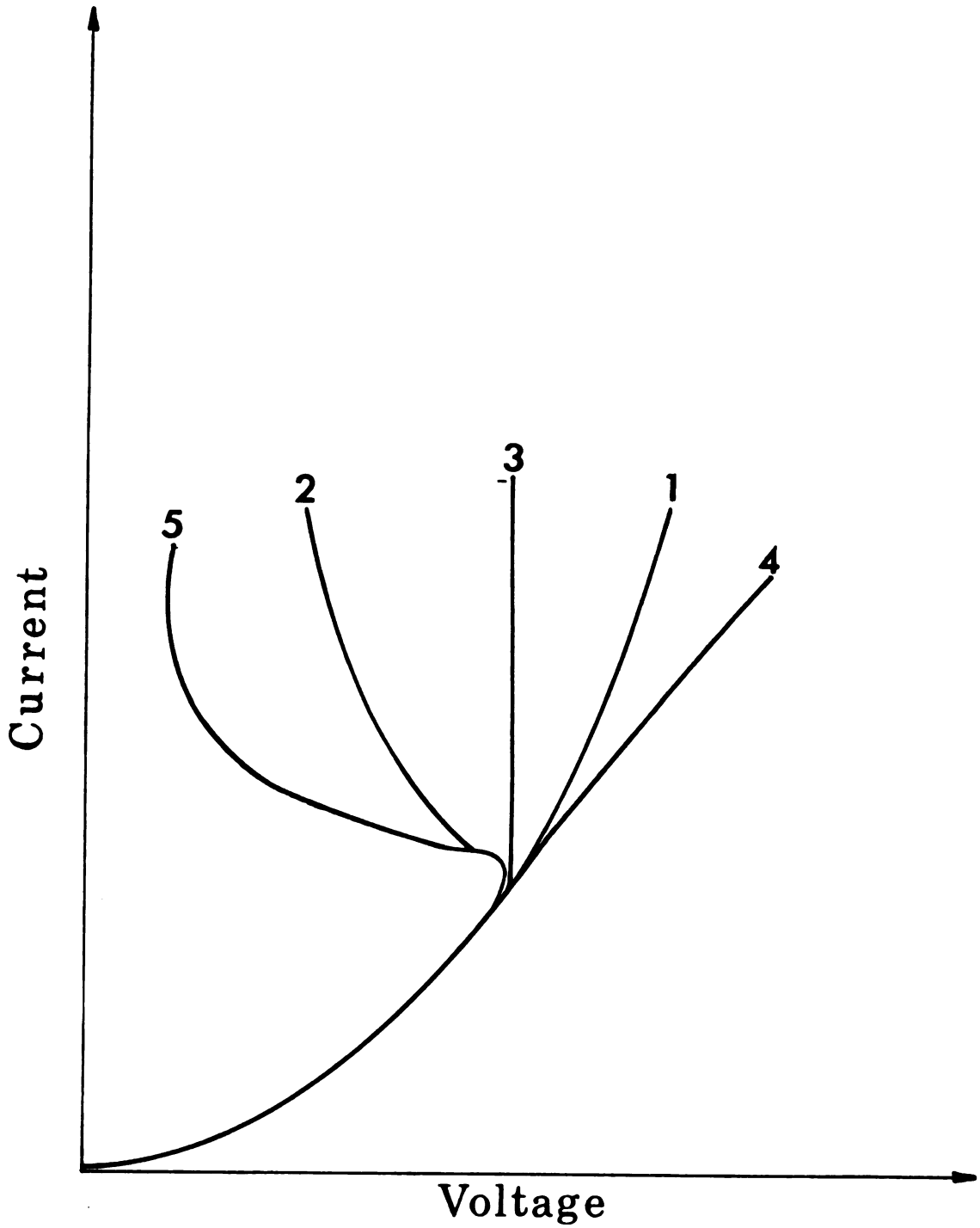

Figure 4. 11. The corresponding I-V characteristic curves for the $\sigma(T)$ dependences shown in Figure 4. 10.

CHAPTER V

CONCLUSIONS

5.1 Summary of the Significant Results

Nondestructive, reversible, current-controlled switching was observed in oxidized vanadium layers prepared using an extremely simple, sample-preparation technique. Inductance effects and current-controlled, negative differential resistance were observed in these oxidized vanadium layers. The inductances were found to be independent of frequency. This lends direct support to the theory developed by Berglund and Walden[3]; they predicted that, if a material could be prepared which possessed no thermal hysteresis effects, then the inductance of the material would be independent of frequency. Our material exhibited no thermal hysteresis effects. Inductances for dc bias currents above and below threshold were measured. For the case of zero dc bias, inductances in excess of 100 mH were observed; however, the Q of the structure was quite low. Also, the observed inductances were found to be strongly dependent upon the dc bias, suggesting

possible applications as inductors and varactors in integrated circuits. Before this phenomena can be used effectively, however, the series resistance problem must be overcome.

The switching-delay-time constants were measured and found to be on the order of 10^{-6} seconds. They were also found to be dependent upon the bias voltage as well as the bath temperature. The threshold voltages required to actuate switching were also measured and found to range from 4 volts to 10 volts, depending upon contact conditions, the dc bias voltage and the ambient temperature.

The thermal-transport equation was solved and an analytical expression for the switching threshold voltage was obtained for the two most important sample configurations. It was found that the threshold voltage for both configurations employed should be proportional to the thermal conductivity but inversely proportional to the rate of change of the electrical conductivity with temperature. In addition, the threshold voltage for the sandwich-type configuration was found to be independent of the layer's thickness while that for the planar-type

configuration was found to be strongly dependent on the film thickness as well as the thickness of the insulating layer. This suggests that the sandwich-type configuration will have a more constant and stable threshold voltage. The other advantage of the sandwich-type configuration over the planar-type configuration is that the inductance effect is independent of frequency over a much wider frequency range. The fact that the threshold voltage is bath temperature dependent suggests possible applications as an thermoswitch. All of the fundamental conclusions of the theoretical development were verified in the laboratory, thereby reinforcing the basic postulate on which the entire analysis was performed: Current-controlled switching in these devices is thermally initiated.

5.2 Suggested Additional Research

Although these oxidized vanadium foils show promise as being compact inductors, varactors and thermoswitches, serious deficiencies still exist with them: namely their large, series resistances, their relatively poor stability and poor reproducibility. These deficiencies are characteristic of virtually

all of the amorphous semiconductors, not just the material selected to investigate here.

Work should be continued in hopes of substantially lowering the series resistance, improving the stability and reproducibility, as well as increasing magnitude of the inductance effects. The following experiments are suggested:

(1) Improvements can be made in the overall switching properties of the devices if, during oxidation, the surrounding environment is more closely controlled, and if after oxidation, the sample is annealed in an inert atmosphere. This will guarantee a more uniform, contamination-free oxidized vanadium layer.

(2) The electrical contacts were relatively noisy, due principally to the crude method in which contact was made between the sample and the electrodes. Evaporated gold layer or alloyed lead-tin contacts should substantially improve the overall characteristics of the devices.

(3) The memory effect observed in amorphous semiconductors has been confirmed to be associated with microscopic structural changes within the material[1].

This change in local order is initiated by the thermal instability resulting in thermal filament formation within the material[1]. In order to provide more information so that one is in a better position to understand the observed switching effects in this vanadium-oxide complex, microprobe techniques should be utilized in order to see if there is thermal-filament formation within the oxidized vanadium layer.

(4) Also, in order to gain a more complete understanding of the observed switching phenomena, determination of the oxidized layer's chemical composition through chemical analysis is suggested.

(5) All the data presented in the discussion section of the previous Chapter have been normalized; this is due to a lack of knowledge of the magnitude of some bulk parameters such as the layer's thermal conductivity, heat capacity, band gap, and so forth. Measurements of the above mentioned parameters are therefore suggested in order to further refine the theory and, consequently, obtain a better understanding of the conduction and switching processes.

(6) The electrical conduction mechanisms in amorphous materials is not well known at this time. Before the switching effects investigated here can ever be completely understood, a better understanding of the

conduction process in amorphous materials is required. A detailed computer analysis, based on the models developed in this thesis, would represent a positive step toward developing a more complete understanding of the switching processes.

APPENDIX

APPENDIX A

RADIUS OF THE RING IN THE X-RAY PICTURES OF PURE VANADIUM FOIL

The characteristic patterns made on photographic film as a result of X-rays inpinging upon solids may be understood in terms of Bragg's law. The Bragg reflection law is

$$2d(h,k,l) \sin \theta = n\lambda, \qquad \text{A.1}$$

where λ is the wavelength of the incident radiation, θ is the reflection angle (see Figure A.1), $d(h,k,l)$ is the distance between the two nearest reflection planes in the solid, n is a positive integer, and h,k and l are the reciprocal lattice constants. For this experiment, the $K\alpha_1$ line from a copper target was selected; consequently[29],

$$\lambda = 1.54 \text{ A.}$$

In order to determine $d(h,k,l)$, one has to first determine which plane reflects the incident X-ray. Vanadium is in b.c.c. lattice structure[29], and the reflection intensity is proportional to the absolute value of the structure factor $S(h,k,l)$. For a b.c.c.

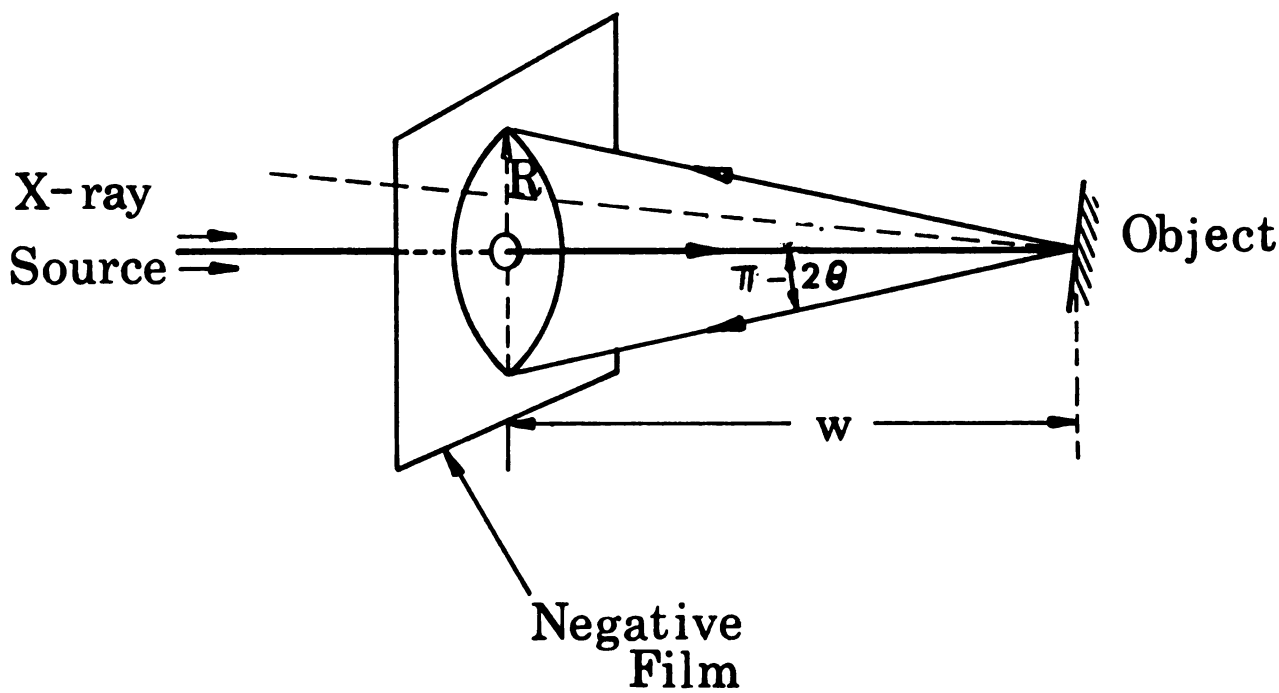

Figure A. 1. Experimental arrangement for making pin-hole back-reflection, x-ray photographs.

lattice, S(h,k,l) is

$$S(h,k,l) = f\{1 + \exp.[-i\pi(h+k+l)]\}.$$

When h+k+l = odd integer, S will be zero, this means no reflection is expected, if h+k+l = even integer, S will be equal to 2f; this corresponds to the maximum reflection condition.

$$\text{Since} \quad d = \frac{a}{\sqrt{1+1+0}} = \frac{a}{\sqrt{2}} \qquad \text{A.2}$$

where a = 3.03A is the vanadium lattice constant at room temperature.

Now, if one let n=1, one has, from Equation A.1,

$$2\,\frac{3.03}{\sqrt{2}}\,\sin\theta = 1.54$$

Therefore,

$$\sin\theta = 0.359$$

$$\theta = \sin^{-1}0.359 = 21°$$

$$2\theta = 42°. \qquad \text{A.3}$$

The distance between the film and the object is W, thus the radius of the expected ring will be

$$R = W \cdot \tan(\pi - 2\theta) = W \cdot \tan 42° = 0.9004W \qquad \text{A.4}$$

APPENDIX B

DERIVATION OF EQUATION 4.23

From Equation 4.22,

$$V_s(x,p) = \frac{A_s}{pq_s^2}\left[1 - \frac{\cosh q_s x}{\cosh q_s \frac{L_s}{2}}\right]$$

$$= \frac{A_s K_s}{P(P-K_s B_s)}\left[1 - \frac{\cosh \sqrt{P-K_s B_s}\ \frac{x}{\sqrt{K_s}}}{\cosh \sqrt{P-K_s B_s}\ \frac{L_s}{2\sqrt{K_s}}}\right]. \qquad \text{B.1}$$

If one lets

$$P - K_s B_s = P' \qquad \text{B.2}$$

and

$$q = \sqrt{\frac{P-K_s B_s}{K_s}} = q'_s \qquad \text{B.3}$$

one will have

$$\frac{A_s}{pq_s^2} = \frac{A_s}{Pq'^2_s} = \frac{A_s K_s}{P'(P'+K_s B_s)}$$

$$= \frac{A_s}{B_s}\left(\frac{1}{P'}\ \frac{1}{P'+K_s B_s}\right). \qquad \text{B.4}$$

Thus

$$V_s(x,p) = V_s(x,p')$$

$$= \frac{A_s}{B_s}\left[\left(\frac{1}{P'}\right)\left(1 - \frac{\cosh q_s' x}{\cosh q_s' \frac{L_s}{2}}\right)\right.$$

$$\left. = -\left(\frac{1}{P'+K_sB_s}\right)\left(1 - \frac{\cosh q_s' x}{\cosh q_s' \frac{L_s}{2}}\right)\right] .$$

or

$$V_s(x,p') = \frac{A_s}{B_s}\left[\left(\frac{1}{P'}\right)\left(1 - \frac{\cosh \sqrt{P'}\,\frac{x}{\sqrt{K_s}}}{\cosh \sqrt{P'}\,\frac{L_s}{2\sqrt{K_s}}}\right)\right.$$

$$\left. = \frac{1}{(P'+K_sB_s)}\left(1 - \frac{\cosh \sqrt{P'}\,\frac{x}{\sqrt{K_s}}}{\cosh \sqrt{P'}\,\frac{L_s}{2\sqrt{K_s}}}\right)\right] . \qquad \text{B.5}$$

The first term in the above equation is then transformed to be [30]

$$\frac{A_s}{B_s}\left[e^{K_sB_st} - e^{K_sB_st}\left(1 + \frac{4}{\pi}\sum_{n=1}^{\infty}\frac{(-1)^n}{2n-1}\, e^{\frac{-(2n-1)^2\pi^2K_st}{L_s^2}} \cos\frac{(2n-1)\pi x}{L_s}\right)\right]$$

$$= \frac{-A_s}{B_s}\frac{4}{\pi}\sum_{n=1}^{\infty}\frac{(-1)^n}{2n-1}\, e^{\left\{K_s\left[B_s - \frac{(2n-1)^2\pi^2}{L_s^2}\right]t\right\}} \cos\frac{(2n-1)\pi x}{L_s} \qquad \text{B.6}$$

The second term is transformed to be

$$-\frac{A_s}{B_s}\left(1-\int_0^t F(U)\,dU\right), \qquad \text{B.7}$$

where

$$F(U) = L^{-1}\left[\frac{\cosh\sqrt{P-K_sB_s}\;\frac{x}{\sqrt{K_s}}}{\cosh\sqrt{P-K_sB_s}\;\frac{L_s}{2\sqrt{K_s}}}\right]$$

$$= \frac{4\pi K_s}{L_s^2}\left[\sum_{n=1}^{\infty}(-1)^{n-1}(2n-1)\,e^{\{K_s(B_s-\frac{(2n-1)^2\pi^2}{L_s^2})t\}}\cdot\right.$$

$$\left.\cos\frac{(2n-1)\pi x}{L_s}\right]. \qquad \text{B.8}$$

Therefore,

$$-\frac{A_1}{B_1}\left(1-\int_0^t F(U)\,dU\right)$$

$$= -\frac{A_1}{B_1}\left\{1-\sum_{n=1}^{\infty}\frac{4\pi}{L_s^2}\;\frac{1}{B_s-\frac{(2n-1)^2\pi^2}{L_s^2}}\right.$$

$$\left[(-1)^{n-1}(2n-1)\,e^{K_s\left(B_s-\frac{(2n-1)^2\pi^2}{L_s^2}\right)t}\cos\frac{(2n-1)\pi\sqrt{K_s}\,x}{L_s}\right.$$

$$\left.\left.+\sum_{n=1}^{\infty}(-1)^{n-1}(2n-1)\cos\frac{(2n-1)\pi x}{L_s}\right]\right\} \qquad \text{B.9}$$

Thus, the temperature $T_s(x,t)$ of the sample is

$$T_s(x,t) = L^{-1}[V_s(x,p)]$$

$$= \frac{\sigma(T_o)}{\sigma_T(T_o)} \left\{ \sum_{n=1}^{\infty} \frac{1}{\frac{L_s^2}{4\pi}\left[\frac{E^2\sigma_T(T_o)}{k_s} - \frac{(2n-1)^2\pi^2}{L_s^2}\right]} \right.$$

$$\left[(-1)^{n-1}(2n-1)\, e^{\frac{k_s}{c_s}\left(\frac{E^2\sigma_T(T_o)}{k_s} - \frac{(2n-1)^2\pi^2}{L_s^2}\right)t} \right.$$

$$\left. - (-1)^{n-1}(2n-1) \right] \cos\frac{(2n-1)\pi x}{L_s} -$$

$$- \frac{4}{\pi} \sum_{n=1}^{\infty} \frac{(-1)^n}{2n-1}\, e^{\frac{k_s}{c_s}\left[\frac{E^2\sigma_T(T_o)}{k_s} - \frac{(2n-1)\pi^2}{L_s^2}\right]t}$$

$$\left. \cos\frac{(2n-1)\pi x}{L_s} - 1 \right\}, \qquad \text{B.10}$$

which is Equation 4.23.

APPENDIX C

DERIVATION OF EQUATION 4.79

From Equation 4.78,

$$\frac{dJ}{dE} = a\sigma_{oa'} + b\sigma_{ob'} + aM_aT_a + bM_bT_b$$

$$+ 2a\sigma_{oa'}\left(1 - \frac{k_i}{S_1S_2M_bE^2}\right)^{-2} \frac{k_iE^{-2}}{S_1S_2M_a}$$

$$+ 2b\sigma_{ob'}\left(1 - \frac{k_i}{S_1S_2M_bE^2}\right)^{-2} \frac{k_iE^{-2}}{S_1S_2M_b}$$

$$= a\sigma_{oa'} + b\sigma_{ob'} + aM_aT_a + bM_bT_b$$

$$+ 2a \frac{k_iM_a}{S_1S_2\sigma_{oa'}} T_a^2 E^{-2} + 2b \frac{k_iM_b}{S_1S_2\sigma_{ob'}} T_b^2 E^{-2}. \qquad C.1$$

If one lets

$$\sigma_{oa'} = \left(\frac{k_i}{S_1S_2E^2} - M_a\right) T_a \qquad C.2$$

and

$$\sigma_{ob'} = \left(\frac{k_i}{S_1S_2E^2} - M_b\right) T_b \qquad C.3$$

one obtains

$$E^{-2} = \left(\frac{\sigma_{oa'}}{T_a} + M_a\right) \frac{S_1S_2}{k_i}$$

$$= \left(\frac{\sigma_{ob'}}{T_b} + M_b\right) \frac{S_1S_2}{k_i} \qquad C.4$$

Substituting E^{-2} into the above expression for $\frac{dJ}{dE}$ (Equation C.4), one obtains

$$\frac{dJ}{dE} = a\sigma_{oa'} + b_{ob'} + aM_aT_a + bM_bT_b$$
$$+ 2a \frac{M_aT_a}{\sigma_{oa'}} (\sigma_{oa'} + M_aT_a)$$
$$+ 2b \frac{M_bT_b}{\sigma_{ob'}} (\sigma_{ob'} + M_bT_b)$$

Combining Equations (4.70) and (4.71) with C.5, one obtains

$$\frac{dJ}{dE} = a\sigma_a + b\sigma_b + 2a \frac{M_aT_a}{\sigma_{oa'}} \sigma_a + 2b \frac{M_bT_b}{\sigma_{ob'}} \sigma_b$$
$$= a\sigma_a\left(1 + \frac{2M_aT_a}{\sigma_{oa'}}\right) + b\sigma_b\left(1 + \frac{2M_bT_b}{\sigma_{ob'}}\right) \qquad \text{C.6}$$

which is Equation 4.79.

BIBLIOGRAPHY

BIBLIOGRAPHY

1. S.N. Mott, "International Conference on Amorphous and Liquid Semiconductors," 24-27 Sept. (1969), Cambridge University.

2. A.F. Loffe, A.R. Regel, "Non-crystalline Amorphous, and Liquid Electronic Semiconductors," A.F. Gibson, ed., Progress in Semiconductors, Vol. 4, London: Heywood and Co., 1960.

3. C.N. Berglund, R.H. Walden, "A Thin-film Inductance Using Thermal Filaments," IEEE Trans. on Electron Devices, vol. ED-17, pp.137-148, Feb. (1970).

4. S.R. Ovshinsky, "Reversible Electrical Switching Phenomena in Disordered Structures," Phy. Rev. Letters, 21:20 (1968), pp.1450-1453.

5. A.H. Clark, "A Refiew of Band Structure and Transport Mechanisms in Elemental Amorphous Semiconductors," J. of Non-crys. Solids, 2 (1970), 52-65.

6. J.G. Simmons, "Applications of Amorphous Semiconductors in Electron Devices," Contemp. Phys., (1970), vol. 11, no. 1, 21-41.

7. David Adler, "Theory Gives Shape to Amorphous Materials," Electronics, Sept. (1970), 61-76.

8. P.J. Walsh, R. Vogel, and E. Evans, "Conduction and Electrical Switching in Amorphous Chalcogenide Semiconductor Film," Phys. Rev., (1969) 178, 1274-1279.

9. K.W. Boer, S.N. Ovshinsky, "Electrothermal Initiation of an Electronic Switching Mechanism in Semiconducting Glagges," J. of App. Phys., vol. 41, no. 6, May (1970), 2675-2681.

10. A.C. Warren, "Switching Mechanism In Chalcogenide Glasses," Electronics Letter (1969) 5, 461-462.

11. R.K. Ridley, "Specific Negative Resistance in Solids," Proc. Phys. Soc., (1963) vol. 82, no. 954-966.

12. M.H. Cohen, "Electronic Structure and Transport in Covalent Amorphous Semiconducting Alloys," J. of Non-Crys. Solids, 2 (1970), 432-443.

13. E.N. Economou, M.H. Cohen, "Energy Bands in One-Dimensional Aperiodic Potentials," Phy. Rev. Letter, vol. 24, no. 5, (1970), 218-219.

14. N.F. Mott, "Conduction in Non-crystalline Systems-- Part 1, Localized Electronic States in Disordered Systems," Phil. Mag., 17:150, June (1968), 1259-1268.

15. H. Fritzsche, "Physics of Instabilities in Amorphous Semiconductors," I.B.M. J. Res. Develop. 13 (1969), 515-521.

16. C.N. Berglund, "Thermal Filaments in Vanadium Dioxide," IEEE Trans. on Electron Devices, vol. ED-16 (1969), May, 432-437.

17. Hisao Futaki, "A New Type Semiconductor (Critical Temperature Resistor)," Japanese J. of App. Phys., vol. 4, no. 1, Jan, 1965, 28-41.

18. F.J. Morin, "Oxides Which Show a Metal-to-Insulator Transition at the Neel Temperature," Phy. Rev. Letter, vol. 13 #1 (1959), 34-36.

19. David Adler, Harvey Brooks, "Transitional Metals Oxide," Phy. Rev., 155 (1967), 851-860.

20. Alpha Inorganics #00394 Vanadium Foil.

21. C. Kittel, Introduction to Solid State Physics, 3rd Ed., John Wiley and Sons, Inc. (1968), Chapter 2.

22. K.W. Boer, R. Haislip, "Semiconductivity of Glasses," Phy. Rev. Letters, vol. 24, no. 5, (1970), 230-231.

23. H.S. Carslow, H.C. Jaeger, Heat Conduction in Solids, 2nd Ed., Oxford Clarendon Press, 1959.

24. K.W. Boer, G. Dohler, "Temperature Distribution and Its Kinetics in a Semiconducting Sandwich," Phys. Stat. Sol. 36 (1969) 679.

25. B.W. Knight, G.A. Peterson, "Theory of the Gunn Effect," Phys. Rev. vol. 155, no. 2, (1967) 393-404.

26. R.E. Burgess, "Negative Resistance in Semiconducting Device," Can. J. Phys. vol. 38, (1960) 369-375.

27. C.R. Wylie, Jr., Advanced Engineering Mathematics, 2nd Ed. 1960, New York, McGraw-Hill.

28. S.R. Ovshinsky, E.J. Evans, D.L. Nelson, and H. Fritzsche, "Radiation Hardness of Ovonic Devices," IEEE Trans. on Nucl. Sci., NS-15 (1968) 311.

29. B.N. Cullity, Elements of X-Ray Diffraction, (1956) Addison-Wesley Co.

30. M.R. Spiegel, Mathematical Handbook, McGraw-Hill, (1968).

31. E.A. Davis and R.F. Shaw, "Characteristic Phenomena in Amorphous Semiconductors," J. Non-crys. Solids 2 (1970) 406-431.

32. Hansen, Constitution of Binary Alloys, 2nd Ed. 1958, McGraw-Hill, Page 806-807, and Page 992-993.

33. A. Sieverts and A. Gotta, Z. anorg. Chem., 172, 1928, 1-31.

34. H. Hahn, Z. anorg. Chem., 258, 1949, 58-68.